FINAL REPORT

on

MODIFIED EUTECTIC ALLOYS FOR HIGH TEMPERATURE SERVICE

for Contract Period

July 1967 to April 1969

Section IV: "Influence of Composition and Cast Structure on the Stress Rupture Properties of Cobalt Base Superalloys"

by

M. U. Ordillas, Jr. and J. F. Wallace

Prepared for

National Aeronautics and Space Administration

Lewis Research Center

Cleveland, Ohio

Division of Metallurgy and Material Science

Case Western Reserve University

10900 Euclid Avenue

Cleveland, Ohio 44106

FINAL REPORT

on

MODIFIED EUTECTIC ALLOYS FOR HIGH TEMPERATURE SERVICE

for Contract Period

July 1967 to April 1969

Section IV: "Influence of Composition and Cast Structure on the Stress Rupture Properties of Cobalt Base Superalloys"

by

M. U. Ordillas, Jr. and J. F. Wallace

Prepared for

National Aeronautics and Space Administration

Lewis Research Center

Cleveland, Ohio

Division of Metallurgy and Material Science

Case Western Reserve University

10900 Euclid Avenue

Cleveland, Ohio 44106

ABSTRACT

Various types of congruently melting phases were selected and tested to determine their properties and feasibility for casting. The better congruently melting alloys were modified with a considerable number of additions to enhance oxidation resistance, provide solid solution strengthening and produce discrete precipitates from the melt. The resulting modified alloys had complex structures. Stress rupture testing was employed to screen these alloys; promising high temperature properties were obtained with the Fe - 50 Co and Co - 15 W base alloys. The microprobe was employed to determine the effects of the various elements on the structure of these two alloys, while metallographic examination of stress rupture test bars was employed to determine the phases associated with failure during testing. Based on these examinations, elements responsible for embrittling phases, those that had little effect or duplicated the influence of more desirable elements were removed. Although chromium did not provide carbide strengthening, it was a potent solid solution strengthener and was increased. This composition modification process was effective in changing the microstructures of the alloys to the desired ones where small discrete precipitates were randomly distributed in the

matrix. The stress rupture properties of the Fe - 50 Co base alloy were not greatly affected but the behaviour of the Co - 15 W base alloy was markedly improved. A faster solidification rate and partial directional solidification, obtained with a chill at the bottom of the heated mold, increased the stress rupture properties of both alloys. Lower mold temperatures plus chilling of the test bar base produced a finer structure and some further improvement in properties. The Co - 15 W, 20 Cr, 2 Zr, 2 Ti, 1 C alloy developed in this study, when cast with a chill at the base of the casting, exhibited stress rupture behaviour comparable to the better nickel-base superalloys.

ACKNOWLEDGMENTS

The sponsorship of this investigation at Case Western Reserve University by the National Aeronautics and Space Administration under Grant No. ~~NsG-639~~ is NGR-36-003-033 acknowledged and appreciated. The contribution of the Ford Foundation, University of the Philippines and Educational Projects, Inc. in providing tuition and financial support for the principal author is also acknowledged.

TABLE OF CONTENTS

Page

LIST OF TABLES

LIST OF FIGURES

INTRODUCTION

The considerable significance of temperature in determining the output of gas turbines makes it desirable to continue to develop high temperature materials with improved properties. This project is concerned with the means of improving the strength of metallic materials used for service at about 1800 F. These are commonly called superalloys. The strengthening techniques employed for superalloys include solid solution hardening, precipitation hardening, dispersion strengthening, directional solidification, and eutectic modification.

The extent of solid solubility varies widely between different combinations of metallic elements. For solid solution strengthening purposes, the most useful alloy systems are those wherein the solubility limits are only fairly wide. If the solubility limit is too narrow, the second phase may precipitate out and cause some loss in solid solution hardening effect. In alloy systems where complete solid solubility in all proportions are observed, the binary elements are so alike in atomic size and chemical properties that hardening effects are negligible.

Recent trends in superalloy development indicate that the common refractory metals are the major elements used as solid solution strengtheners. The refractory

metals have very high melting points and exhibit wide solubilities in the nickel, cobalt and iron superalloy base elements currently used. Unfortunately, the refractory metals oxidize quite readily at high temperatures (1)* and may decrease the oxidation resistance of the base element. Further, these are generally heavy and may increase alloy density--an important consideration in aerospace applications. In an iron base alloy it was determined that the effect of combined additions of the refractory elements was greater than the sum of the contributions of the individual elements (2). The better properties of the more complex alloys have been attributed to more effective keying of grain boundaries by mixtures of solute atoms of different sizes (3). Thus the composition of superalloys have become more complex and these alloys may contain 8 to 12 intentionally added alloying elements. Unfortunately, 12 intentional additions also introduce 12 reasons why a melt can be off-specification.

Precipitation hardening has been, and still is, the major mode by which commercial superalloys are strengthened. The most important factor responsible for the high temperature strength of the widely used nickel superalloys is the precipitation of a second phase--the Ni_3Al intermetallic compound gamma prime (4,5). The exact

---

* The numbers in parentheses refer to the bibliography at the end of the thesis.

mechanism by which it effects strengthening is not entirely established but it has been hypothesized that the major strengthening effect of the precipitate is not from coherency strains but a result of a difference in flow characteristics between two phases (6).

If the major effect stems mainly from particle size, interparticle spacing, and uniformity of distribution of a strong hard particle in the matrix, then any strong and stable precipitate or dispersion may provide the requisite high temperature strength. If this effect applies generally, it should be possible to strengthen other matrix materials similarly regardless of how the dispersion is introduced. This type of behavior has been demonstrated by the various dispersion hardened alloys that have recently developed, such as the SAP alloys (7) and TD-nickel (8) used for extending the high temperature capabilities of aluminum and nickel. Dispersion hardening has also been applied in an attempt to improve the strength of nickel-base (9 -12) and cobalt-base (13,14) alloys in the temperature range where conventional superalloys are commonly used.

The dispersion hardened materials are commonly produced by powder metallurgy methods. The technique has inherent difficulties such as non-uniformity of dispersions, bulky equipment, and limited size and shape of

products. It is therefore desirable to find other means of introducing the dispersion. Internal oxidation has been attempted but has problems including limited selection of alloy systems, complications in alloying to allow introduction of the oxidant, and the control of dispersion size and distribution (15-20). Dispersions that harden effectively at high temperatures must be fine, uniformly distributed and have a small mean free path (21-23). Precipitation hardening has been successful in meeting these requirements and is widely employed. It also appears feasible to introduce these precipitated particles from the melt. It has been demonstrated (24) that stable nitride dispersions of about 0.1 micron size can be introduced into high purity chromium melts.

Carbides precipitate from the melt in a variety of shapes, sizes, compositions and distributions that may be beneficial or harmful. Uncontrolled, the carbides can grow to large sizes, segregate to delineate regions of weakness, or form deleterious structures. However, the variety of sizes, shapes, compositions and distributions can also be taken as an indication that with judicious selection of alloy systems and proper control, carbides could precipitate to provide considerable strengthening. One of the objectives of this investigation is to attempt to produce an alloy with excellent high temperature proper-

ties strengthened with carbides precipitated from the melt.

The strengthening phases in precipitation hardening return to solution at the solvus. Since the solvus is generally well below the melting point of the alloy, precipitation hardened materials cannot take full advantage of the melting point of the alloy. Theoretically, precipitation hardened alloys can be used to the solvus temperatures. However, they lose their strength well below the solvus temperature. On the other hand, phases that form during solidification in cast materials may be stable and at least theoretically capable of retaining their strength to close to the melting point. Some recent work designed to take advantage of this fact involved modification of eutectic alloys (25-27). Eutectic modification as applied to high temperature materials was conceived because of the success of the technique on materials used at lower temperatures in changing coarse eutectic structures into fine precipitates (28,29). The aforementioned studies did show that an alloy with superior high temperature properties could be obtained from a modified eutectic alloy. The modification resulted in the replacement of the continuous or platelike constituents with equiaxed or discontinuous phases.

It has been observed that failure of stress rupture specimens occurred at grain boundaries transverse to the direction of application of stress (30). It became apparent that if the number of grain boundaries were reduced by increasing the grain size or if the grain boundaries were aligned with the direction of stress, an improvement in mechanical properties would result. It has been demonstrated (31) in an investment cast stellite type alloy that, by simply increasing mold temperature, coarser grained castings with decidely improved stress rupture lives could be obtained.

A special precision casting technique has been developed, based on directional solidification, to prcduce columnar grains parallel to the major axis of gas turbine components thus eliminating grain boundaries transverse to the direction of stress (30,32-35). Tests on the castings showed superior strength and ductility at both room and high temperatures over conventionally cast components. Directional solidification has also been applied to eutectics with some limited success (36). Examination of the cast structure revealed that: (a) primary dendrites were aligned properly but the secondary dendrite arms grew transverse to the direction of stress; and (b) considerable segregation during solidification caused eutectic phases to form within the interdendritic zones.

Eutectic alloys have the advantage of a single solidification temperature and good casting properties, although rapid cooling on the presence of additional alloys can markedly affect this behavior and can cause considerable segregation during the formation of pro-eutectic phases (36,37). To minimize dendritic segregation in eutectic alloys, an alloy with very little tendency to be affected by small changes in composition and cooling rate is preferred.

Congruent melting phases appear to offer the possibility of minimizing segregation and a single melting temperature, since the liquid and solid in equilibrium with it have the same composition. Their solidification is similar to that of pure metals. Many congruently melting phases have very extensive solid solubilities, especially at the higher temperatures, and some of these alloys exhibit limited solubility or ordering at lower temperatures. These phases exist in various crystal structures, from simple to complex. These facts suggest that a variety of strengthening mechanisms exist for these alloys. Accordingly, another objective of this study is to investigate the feasibility of using congruently melting phases as base alloys for high temperature cast superalloys.

Some high temperature alloys have been developed by an empirical process involving the making and testing of hundreds of alloy combinations, the effort finally culminating in the selection and refinement of the best in the series. Because of the growing complexity of these alloys, means of decreasing the number of experiments is very desirable. By necessity, statistical methods had to be used to analyze the hundreds of alloys tested. A natural consequence of this is the extension of statistics to the design of the experiments themselves. Statistically designed experiments allow the simultaneous variation of the type and quantity of alloying elements and an accurate evaluation of results from fewer alloy combinations. This technique employing the Latin Square and fractional factorial designs has been employed in the development of one of the strongest experimental cast high temperature alloys (4,6,38,39). To minimize the number of alloys, a technique that involves subtracting the amount of material that goes into the precipitation of strengthening phases from proposed alloy compositions has been employed (5). If the mean electron density number calculated for the residual material exceeds a certain value, it is predicted that the proposed alloy is prone to the formation of embrittling phases and therefore need not be studied

further. The predictions of this method provided excellent correlations with observations on the presence of embrittling phases in existing alloys.

In developing the alloy series examined in this study, the microprobe was employed to eliminate undesirable phases. In this technique, the starting point is a complex alloy loaded with all the alloying elements expected to impart strength. The cast structure is examined and the presence of embrittling or undesirable phases noted. The elements mainly responsible for these undesirable phases or structures are then identified with the microprobe. Removal or reduction in the amount of such elements may then result in improved properties. This technique is the reverse of the usual practice of adding more and more elements to the base alloy until a good combination is obtained.

MATERIALS AND PROCEDURE

In searching for a suitable alloy base for more detailed investigation, binary alloys which melted congruently at temperatures above 1,200 C were chosen from available phase diagrams (40). These alloys are listed in Table I. The selection is varied to allow representative alloys which may be strengthened by solid solution strengthening, precipitation hardening, strengthening through ordering, or hardening through complex mechanisms in a complex crystal structure. Although minimum melting point phases were preferred, maximum melting point phases were also included in the study.

Elements that imparted oxidation resistance, solid solution strengthening, or produced dispersed phases were selected as modifying elements. For oxidation resistance, Cr, Al and Si were used; Zr, Ti, C and B were selected to provide carbides and borides; finally for solid solution strengthening, elements with high solid solubility in the binary elements (preferably refractory metals) were selected. The physical properties of the base elements and the alloying elements are listed in Table II. High purity materials of the form and purity listed in Table III were used as melting stock. The quantities of modifying elements added were sufficiently large to insure that their

effects or distribution in the alloy could be detected. In a previous study on modified eutectic alloys (27), it was found that a (Zr + Ti)/C ratio of 0.76 appeared to be an optimum ratio when these elements were used together. Accordingly, this ratio was utilized in this work.

A small MRC (Materials Research Company) laboratory vacuum arc furnace, equipped with a water-cooled copper hearth, was used to melt and cast-in-place the exploratory alloys in 1/2 atmosphere of gettered argon. The castings were in the form of bars 1/4"x1/2"x4" long. To improve the distribution of elements in the buttons, they were remelted three times. The arc-melting and casting-in-place process subjected the alloys to a severe chill and these solidified rapidly in a high thermal gradient. The binaries which cracked during this solidification and cooling process were considered unsuitable and not studied further.

The following melting practice was followed in producing the as-cast stress rupture test bars. Heats of 180 cubic centimeters were induction melted in a 960 cps furnace and stabilized zirconia crucibles surrounded by a graphite susceptor. A few pieces of coarse melting stock and the Zr and Ti sponge were loaded into separate charging bins;

the remaining charge material and melting stock was packed into the crucible and later inserted into the susceptor. All powdered melting stock were pre-mixed before packing into the crucible. The chamber of the vacuum furnace was first evacuated to a pressure of 20 microns Hg. It is then backfilled with argon to -25 psig and re-evacuated to about 30 microns Hg. During the re-evacuation process, sufficient power was placed on the induction coil to produce a barely discernible glow in the charge. The backfilling with argon, re-evacuation, and application of increasing power to the induction coil was repeated 5 times. On the fifth repetition, the charge was reaching the melting point. The chamber was finally backfilled with argon to 1/2 atm and held at this vacuum. Higher power levels to melt and superheat the charge was then applied.

When the charge melted, its temperature was rapidly increased to approximately 250 degrees F superheat as measured by optical pyrometer. The Zr and Ti were then added successively and rapidly. When all the Zr and Ti were dissolved, the rest of the melting stock was added. The larger pieces of melting stock reduced the temperature appreciably and usually did not melt immediately but rather churned or tumbled in the melt for a few seconds.

During this time more power was applied to increase the churning action and raise the temperature. The melt was poured as it attained pouring temperature. The time expended from the start of actual melting to pouring of the melt ranged from 8 to 12 minutes.

The casting was allowed to cool down to about 200 F before the chamber was opened. Test bars were sectioned from the casting, sand blasted and tested at elevated temperatures. The mechanical property measured to evaluate the high temperature properties of the alloys was constant-load stress-rupture life. Test temperatures were maintained at 1850 F $\pm$ 5F in an air atmosphere.

Checks on melting points were made by means of Pt - Pt 10% Rh immersion thermocouple. After filling the mold with molten alloy, the crucible was returned into an upright position and the melt temperature followed by the optical pyrometer. At the appropriate pyrometer reading, the thermocouple is immersed and the temperature measured versus time. A typical thermal analysis curve is shown in Figure 1. The melting points of the alloys were usually close to the temperature capabilities of the quartz protection tube and insulators and higher than the guaranteed reliable readings for the thermocouple. If the thermocouple is inserted too soon at too high a

temperature, the protection tube is weakened considerably and eventually fusing of both thermocouple and insulators occurs. Because of these difficulties the reported melting temperatures should be considered as approximate.

The molds and mold furnace used and the procedure for making conventionally- and directionally-cast test bar clusters were the same as those used in a previous study (36). The mold furnace was modified slightly to permit assembly and dis-assembly inside the vacuum chamber and to facilitate the raising and lowering of the chill block in the furnace chamber. Figure 2 illustrates how the molds were set in the mold furnace. The depth to which the copper chill block is set in the refractory bottom of the mold furnace and the temperature maintained in the mold furnace chamber determined the steepness of the temperature gradient in the mold.

Two sets of samples were initially prepared for microprobe examination. For one set, two short pieces were cut from the middle of the gage section of untested stress rupture bars. One piece was ground to expose the longitudinal section. Both pieces were then mounted in copper-filled diallyl phthalate mounting powder. The mounted samples were ground, polished with 3 micron diamond abrasive, and examined in the unetched condition. The

other set was made by cutting off two short pieces from ruptured test bars and prepared the same way as the first set. The piece sectioned longitudinally always contained the ruptured surface. Comparison of the two sets showed that tested specimens were essentially the same as untested specimens. Except for oxidation of the surface, no effect of long time exposure to 1850 F could be detected in the alloys. Subsequently, untested specimens were no longer prepared.

An MAC (Materials Analysis Company) Model 400 electron microprobe was used for microprobe analysis. Light element analysis was conducted at an electron accelerating voltage of 7.5 KV and a specimen current of 0.20 microampere; heavy element analysis was made at 25 KV and 0.03 microampere specimen current. Light element analysis always preceded heavy element analysis because the beam deposits a thin film of material on the specimen surface which, if too thick, interferes with light element analysis.

Using the microprobe in the x-ray modulation mode, x-ray images of the elements were obtained to show the semi-quantitative distribution of the elements in the various phases in the alloy. A more quantitative description of this distribution was obtained from static

probe analyses of selected areas. The following procedure was followed to obtain the static probe analyses. The instrument was first tuned to the element spectral line desired. The background and peak intensities were then measured from the standard for a given accelerating voltage and specimen current. The desired area to be examined was then quickly swung under the beam and the peak and background for the same spectral line measured. The standard was returned to the beam and again the peak and background measured. The return to the standard was a check to be assured that all readings were taken at the same conditions. Intensities were counted either for 1 second or 5 seconds, depending on whether the line intensity was strong or not. Direct comparisions between the two net intensities were then made. No corrections for fluorescence or absorption were attempted since the alloys in this study are sufficiently complex to make corrections very difficult and hazardous.

Before mounted specimens were examined under the microprobe, they were subjected to microscopic examination. When etching was required, a solution of 100 cc HCl, 50 cc HNO_3, 50 cc H_2O, and 10 cc of 30% H_2O_2 was used. This etchant was more effective if a stock solution of aqueous HCl-HNO_3solution were prepared ahead and drops of hydrogen

peroxide added later as needed.

Secondary dendrite arm spacings and number of precipitates intersected by a line of specific length were measured with a filar eyepiece calibrated against a micrometer. To determine the size distribution of the precipitates, photomicrographs of a micrometer and the specimens were taken at magnifications of 100X and 500X. The pictures were then enlarged a similar amount. Based on the pictures of the micrometer, square reference grids of increasing size were then inscribed on a sheet of clear acetate. The side of the smallest square grid was equivalent to 0.0008 mm or 0.8 micron long. This length was taken as the unit of measurement. Thus each square in reference grid No. 1 had dimension of 0.8 micron x 0.8 micron and an area of 0.64 square micron; in reference grid No. 2, the length of each side was 2 x 0.8 microns; in reference grid No. 3, 3 x 0.8 microns; and so on. The area occupied by the precipitate was estimated by superimposing the reference grids upon it. The reference grid equal to or slightly larger than the precipitate size was reported as the precipitate size. The size distribution data allowed the calculation of the arithmetic mean precipitate size and the volume fraction of precipitates in the alloy. The mean free

path (MFP) was then calculated from the equation

$$MFP = (1 - V_p)/N$$

where V_p is the volume fraction of precipitates and N equals the number of precipitates intersected per unit length (41).

The specimens employed to determine oxidation resistance were slices about 0.05 inch thick from the 3/4 inch central downgate of the cluster castings. They were polished with 600 grit sandpaper and washed with methanol prior to scaling. Some specimens were subjected to static oxidation tests at 1850 F in still air in a muffle furnace. Others were suspended on one arm of a magnetically damped chainomatic analytical balance by a fine nichrome wire in a vertical tube furnace and their weight gain observed with time. The temperature inside the furnace was maintained at 1850 F $\pm$ 3 F. The nichrome suspension wires were carefully measured and cut to the same lengths. Care was made that the same lengths of wire were exposed inside the furnace and that the specimens were placed at the same position in the furnace at each test. Oxidation test on the nichrome wire itself showed that its weight change was negligible compared to those of the specimens.

RESULTS AND DISCUSSION

Exploratory Unalloyed Binaries

The goal of this phase of the investigation was to determine alloy bases that have a potential of improvement by suitable changes in composition and cast structure. Table IV lists the basic compositions and hardnesses of arc-melted exploratory binary alloys. Their corresponding microstructures are shown in Figures 3 and 4. Magnifications of 100X and 250X were employed as required to illustrate the structure. The Fe - 30 Ti, Fe - 45 Cb, Mn -10 Mn - 10 Fe, and Cr - 15 Si alloys were too brittle to be ground and polished satisfactorily. This extreme brittleness prevented reliable hardness testing. This brittleness also eliminated these alloys from further considerations.

The Fe - 65 Ni, Fe - 22 Cr, Fe - 50 Co and Co - 15W alloys were single-phased--indicating that they probably solidified in the expected congruent manner. Their hardnesses were low, from a high of 23 R_C for Co - 15 W to a low of 0 R_C (81 R_B) for Fe - 65 Ni. Nevertheless, except for the Fe - 65 Ni binary, they were judged to be suitable for further study. Both Ti - 47 Cr and Fe - 34 Mo binary alloys have Widmanstatten-like microstructures.

This probably occurred because two-phase fields exist only 50 F below their melting points. The Ti - 47 Cr binary had a hardness of 56.78 R_C and passable ductility while the Fe - 34 Mo binary had a hardness of 60.00 R_C and good ductility. These hardnesses are exceptionally high for binaries and these two binaries were studied further in the alloyed condition. The Cr - 20 Mo binary was also studied further for its high hardness and passable ductility.

Although the Fe - 37.5 Ti alloy is not a congruently melting composition, it was included to determine the hardening effects of the peritectic reaction on the binary alloy. The hardness of 62.10 R_C for this alloy was the highest among the binary alloys. Thus, the reaction can be considered a potent hardening reaction. This hardness was not compared with the hardness of the congruently melting Fe - 30 Ti binary because of the latter's brittleness. It was noted that while the Fe -30 Ti binary cracked severely while cooling in the copper hearth, the Fe-37.5 Ti binary did not. Its exceptional hardness and passable ductility qualified the Fe - 37.5 Ti binary for further study in the alloyed condition.

Exploratory Alloyed Binary Alloys

The compositions and observed properties of the selected binaries when fully alloyed for solid solution strengthening, oxidation resistance and for production of precipitates from the melt are listed in Table V. The high Ti content alloys were all brittle and either fractured when dropped on the floor or cracked while the investment mold was being removed. Alloying seemed to aggravate the brittleness of these alloys and therefore this group was considered as unsuitable for additional study.

Both the alloyed and unalloyed Fe - 34 Mo alloys oxidized severely. Unalloyed, a thick grey scale was formed; alloyed, the scale was thicker and had a bubbly or mottled appearance. The rapid growth of the scale corresspondingly decreased the load carrying cross section of the test bars. Thus, even if the material was strong, the rapid decrease in cross-sectional area caused stresses to increase resulting in the rupture of the specimens in a short time when tested in air. This alloy was eliminated because of its poor oxidation resistance.

As indicated in Figure 5, the Fe - 15 W base and the Fe - 22 Cr base alloys have similar microstructures and deformation behavior. These figures show the cast structure and the deformed structure after stress rupture testing. At 1850 F, test bars of both alloys elongated as fast as the load was applied. Reductions in diameter were practically uniform throughout the gage length. Necking and fracture occurred when the cross-section was already too small to support the load. Total elongations in both alloys were about 200 %. A similar deformation behavior was previously observed by Vishnevsky (36) in extruded modified Co - 35 W base alloys, and he subsequently found these to exhibit superplastic behavior. This suggests the possibility of finding superplastic behavior in the Fe - 15 W and Fe - 22 Cr alloys. This study, however, does not include examination of this phenomenon.

In these two alloys, the matrix apparently retained the low hardness of the unalloyed state. The precipitates apparently had a negligible strengthening effect. The eutectic structure, which spreads to wide areas, may be expected to have some strengthening effect. However, the eutectic structure also deformed with the matrix and broke up into stringers aligned with the

direction of flow. These stringers eventually served as regions of weakness where cracks initiated and grew. These cracks tended to skirt the discrete precipitates.

Only the Co - 15 W base and the Fe - 50 Co base alloys showed promise among the fully alloyed exploratory alloys. These two were analyzed more closely and are discussed in the following sections.

The Exploratory Fe - 50 Co Base Alloy

The microstructure of this alloy, shown in Figure 6, is composed solely of discrete precipitates which occur in two separate sizes randomly distributed in the matrix. The large-sized precipitates assumed a straight-sided, equiaxed morphology averaging 20 microns across; the smaller precipitates are much more numerous and are about 4 microns in size. The precipitates do not appear to be part of a eutectic structure and no eutectic structure was observed. Optically, all the precipitates appear to have the same identity.

The precipitates apparently served as the location of crack or void formation during stress rupture testing. Figure 6-b shows the void formation in the region near the fracture surface of fractured test bars. The voids appear to form in the interface between the precipitates and the matrix at surfaces perpendicular to the applied

stress and grow in the direction of stress application. This preferential location of void formation in the alloy agrees with the location of maximum tensile stresses between the matrix and a spherical particle shown in Figure 7 as analyzed by Goodier (41). This analysis for spherical particles in an elastic matrix apparently also applied to this system of cubically and irregularly shaped particles.

Since small precipitates predominate in the microstructure, more voids exist near small precipitates. However, the voids adjacent to the big precipitates grew to much larger sizes. This indicates that a size effect on the magnitude of maximum stresses exists such that the larger precipitates probably reduce strength and ductility. As Figure 7 shows the largest tensile stresses occur at the 90 degree pole of a void as soon as the void is formed. These tensile stresses enlarge the void further and ultimately cause fracture.

To obtain an idea of the effects of the various alloying elements on the microstructure, two procedures were employed on the microprobe. X-ray images of the various alloying elements were taken and static probe analysis of the alloy at selected areas were made.

The data obtained are shown in FIgures 8 to 10 and Table VI. The x-ray images show semi-quantitatively how the elements were distributed among the phases in the alloy. The static probe analysis quantifies this distribution. With these data, the following observations were made:

(a) Tungsten was added for strengthening the matrix. However, this element segregated to the discrete precipitates so that only a small percentage remained in the matrix. This indicates that the strengthening effect of W on the matrix is not fully realized in the presence of Ti, Zr and C.

(b) Nearly all of the Cr and Si remained dissolved in the matrix. Although these elements were added specifically for oxidation resistance, these probably also contributed to the strengthening of the matrix. This effect might be enhanced by larger additions of these elements. However, since it was desired to simplify complex systems and obtain the desired properties, Si was eliminated and only Cr was employed in increased amounts in the next alloy.

(c) Practically all of the Zr and Ti segregated to form two types of precipitates in the alloy. These are Ti-rich and Zr-rich carbides. All of the large

sized precipitates were found to be Ti-rich. The composition of both precipitates approximate an MC type carbide and contain very little Co, Fe, Cr or Si. The Ti-rich precipitates are much higher in W content than the Zr-rich precipitates but the concentration of carbon is approximately the same in each. The occurrence of the Ti-rich precipitates in the large sizes and their idiomorphic shapes suggest that these carbides precipitated while the melt was still at very high temperatures.

Since the large Ti-rich precipitates apparently caused eventual fracture, the elimination or at least reduction of their size appeared desirable. Their size can be controlled either by reducing the amount of precipitating material or the apportunity for growth. Thus, in the next alloy cast, the amount of Ti added was reduced from 2 w/o to 1 w/o and at the same time, the solidification rate was increased to reduce growth time. The final alloy composition, modified as noted above, is as follows: Fe - 50 Co Base - 81 w/o, Cr - 10 w/o, W - 5 w/o, Zr - 2 w/o, Ti - 1 w/o and c - 1 w/o.

Exploratory Co-15 W Base Alloy

The other exploratory alloy which showed promise for elevated temperature use was the Co - 15 W base alloy. As

shown in Figure 11, the microstructure is composed of discrete precipitates and a eutectic structure randomly distributed in the matrix. As will be shown shortly, the precipitates occur in two types as they did in the Fe - 50 Co base alloy: a Ti-rich precipitate and a Zr-rich precipitate. The Ti-rich precipitates also have straight-sided, equiaxed morphology with an average size of 10 microns; the Zr-rich precipitates are more irregularly shaped and average 6 microns in size. This indicates that the Ti-rich precipitates probably formed earlier during the solidification.

Examination of the region close to the fracture surface (Figure 11-b) indicates that voids were initiated at the zero degree pole position with respect to the applied stress just as in the Fe - 50 Co base alloy. All the voids or cracks were found only in the matrix and eutectic structure or adjacent to the precipitates. Even though the relief of the eutectic structure from the matrix indicates that it is harder than the matrix, the voids apparently grew into the eutectic structure. This may indicate that the eutectic is brittle.

Necking of the specimen in the fracture zone was very slight, indicating that the specimen fractured in a brittle manner. Plastic flow was necessarily small yet,

as Figure 11-b shows, it effectively broke up the eutectic structure from its usual plate-like morphology into very fine and roughly spheroidal particles. This fracture of the eutectic structure and the growth of the voids indicate that the eutectic structure is not contributing to the strength of the alloy, was brittle or weak as previously mentioned and for this reason should be reduced or eliminated.

Since the formation of phases in an alloy system is primarily a function of composition, knowledge of the distribution of these elements should be helpful in optimizing the structure. The element or elements which preferentially segregate to a certain phase may be considered as responsible for the appearance of that particular phase. The electron microprobe, used in the x-ray modulation mode, yielded the x-ray images in Figures 12-14 and show how the elements distributed among the phases in the alloy. A selected area static probe analysis, listed in Table VI, yielded a more quantitative description of this distribution. These data, obtained with the microprobe, permits the following observations:

(a) Two types of precipitates occur--a Ti-rich precipitate and a Zr-rich precipitate. No Cr-rich discrete precipitate was located. In fact, the Cr con-

centration decreased to very low values at all the discrete precipitates. A similar observation was made earlier in the Fe - 50 Co base alloy. The compositions of these precipitates, as shown in Table VI, correspond to MC type carbides.

(b) Only Cr and Si, of the elements added, preferentially remained in solution with cobalt to form the matrix phase. The other elements segregated to either the discrete precipitates or to the eutectic phase. These observations were interpreted to mean that Cr performed no significant contribution as a carbide strengthener but provided solid solution strengthening in addition to its recognized contribution to oxidation and corrosion resistance. Silicon follows the same distribution as Cr and may be said to act similarly to Cr.

(c) Molybdenum and boron segregated primarily to the eutectic areas. It will be noted that, with the exception of Mo and B, the same alloying elements were used in the Co - 15 W alloys as in the Fe - 50 Co alloy, yet the Fe - 50 Co base alloy does not contain any eutectic structure while the Co - 15 W base alloy shows extensive eutectic structure formation. This suggests that Mo and B may have been responsible for the production of the eutectic structure. If this is so, then the elimination

of Mo and B should reduce or eliminate this eutectic.

Oxidized specimens of this Co - 15 W base alloy exhibited an outer scale which spalled off completely as the specimen cooled down, and a thin green inner scale which was very weakly adherent to the metal. The outer scale has the appearance of faceted crystals. The microprobe analyses of both scales are listed in Table VI. On the outer scale, only Co and oxygen were determined to be present. In the inner scale, the analysis varied greatly from one area to another; in some areas only Co and Cr could be detected while in other areas all the elements, except Zr, were detected. Zirconium was not located in the inner scale. This variation in composition in the inner scale is probably an indication of the variation in oxidation rates of the phases in the alloy during the initial stages of oxidation. The oxidized surface of the large void at the top of Figure 11-b and the oxidized fracture surface at its lower right side show some indication of the variation of oxidation rates of the phases. The unaffected carbide precipitates are surrounded by oxidized material. This alloy did not exhibit the preferential oxidation of carbides usually found in Co-base alloys.

On the basis of the foregoing observations, the alloy composition was simplified by excluding Mo, Si and B from subsequent castings. Molybdenum and boron were removed because these elements were apparently responsible for the formation of the embrittling eutectic structure. Chromium and silicon were added to enhance oxidation resistance and as solid solution strengtheners. Since Si was found to simply duplicate the action of Cr, it was removed and the Cr content was increased from 5 w/o to 10 w/o. The combination of Zr, Ti and C appeared to produce the desired discrete precipitates, so these were retained in the same amounts and proportions. On a weight percent basis, the resulting simplified composition of the next alloy studied was: Co - 15 W base - 85%, Cr- 10%, Zr, - 2%, Ti - 2%, and C- 1%.

Modified Fe - 50 Co Base Alloy

Modification of the exploratory alloy composition by reduction of Ti content and increase in Cr content eliminated the large sized Ti-rich precipitates in the modified Fe - 50 Co alloy. As show in Figure 15, the size was more uniform and reduced to about 5 microns. The literature states that for a dispersion to be an effective strengthener at elevated temperatures, it must

have a small size (although smaller than 5 microns), uniform distribution, and small mean free path in the matrix (20,43-46). Since the average particle size has been reduced, this modified alloy was expected to exhibit better stress rupture life than the exploratory alloy. However, the results of stress rupture tests listed in Table VII and summarized in Figure 16 show that the modification of the Fe - 50 Co alloy reduced, rather than improved, the elevated temperature properties.

Since the average precipitate size of 5 microns in this alloy is still large compared to the usual size range of 0.01 to 1.0 microns employed in other dispersion hardened materials, an attempt was made to decrease the precipitate size. This was undertaken by increasing the solidification rate, since the carbides were precipitated from the melt. The cooling rate was increased, and the castings still properly fed, by chilling the bottom of the casting with a water-cooled copper block as shown in Figure 2-b. This resulted in a partially, but certainly not completely, directionally solidified structure illustrated by the macrostructure in Figure 17-d. This type of structure is referred to as directionally solidified in subsequent sections, although it is not completely directional in its grain growth

pattern. A completely directional solidification was only achieved in one case that is discussed in the last section of this report.

The use of the chill block did achieve a refinement in the size of the precipitates and, as Figure 16 shows, this was accompanied by an improvement in stress rupture life. This improved stress rupture life, however, was still much lower than that of the complex exploratory alloy. Further work with this phase of the study was discontinued because attention was focused on the better properties of the Co - 15W base alloy.

Modified Co - 15 W Base Alloy: Conventionally Cast

A prime consideration in the modification of the Co - 15 W base exploratory alloy was the elimination of the lamellar eutectic phase since this was contributing to embrittlement. The modification consisted of simplifying the composition by excluding Mo, B and Si but doubling the Cr content from 5 w/o to 10 w/o. Figure 18 shows that this modification of the alloy content successfully eliminated the lamellar eutectic structure (compare with the structure in Figure 11). The resulting microstructure is composed solely of discrete precipitates uniformly distributed in the matrix with an average size of 3.5 microns.

The results of stress rupture tests on this modified alloy, assummarized in Figure 19, show that an improvement in elevated temperature properties was realized. The stress for a 100-hour life at 1850 F improved by a factor of 1.8 from 9,000 psi to 16,000 psi. In terms of stress rupture life at 1850 F and 17,500 psi, the improvement is a factor of 24.8--from 1.9 hours to 47 hours. Figure 19 also shows that these properties are comparable to those of commercial Co-base alloys as typified by the alloy SM 302 (48).

The improvement in properties may be attributed to the combined effects of the increase in chromium content, the elimination of the eutectic phase by removal of the molybdenum and boron, and the refinement in precipitate size with the more rapid solidification. The disposition of elements in the alloy is shown in Table VIII and Figures 20 and 21. Except for the absence of segregation of elements to eutectic regions, the distribution of elements among the different phases is essentially those of the exploratory alloy. The inc eased addition of Cr has proportionately increased the amount of Cr dissolved in the matrix. This strengthened the matrix and, as Figure 22 shows, improved the oxidation resistance considerably. As in the exploratory alloy, serious spalling of the outer scale occurs whenever the alloy is cooled. This prohibits

the alloy from being used where thermal fluctuations occur.

In the exploratory alloy, the eutectic phase fractured and served as regions of weakness. Since Cr and W (together with Mo and B) were principal elements in this phase, the elimination of the lamellar structure not only removed the regions of weakness but also liberated some amounts of Cr and W and improved oxidation resistance and solid solution hardening.

Another probable reason for the improvement in properties is the reduction in precipitate size from 8 microns in the exploratory alloy to 3.5 microns in the modified alloy. The refinement in precipitate size is probably also a direct result of the elimination of the eutectic phase. Tungsten preferentially replaces Ti rather than Zr in the carbide precipitates. The liberation of W from the eutectic phase made additional W available for replacement of both Ti and Zr in the carbides. The increased W content in the carbides have changed these from MC type to M_2C approximate composition carbides. Since the melting points of the carbides of W are lower than those of the carbides of Zr and Ti, tungsten probably lowered their melting points proportionately. Accordingly, precipitation occurred at a later stage of the solidification process.

Modified Co - 15 W Base Alloy: Directionally Cast

Modification of the composition, as has been discussed, already resulted to some refinement in precipitate size. However, this size was much larger than those found in the usual dispersion hardened materials. It is therefore desirable to refine this size further. As with the Fe - 50 Co base alloy, further refinement of precipitate size was attempted by chilling the lower end of the casting, thereby increasing the solidification rate and providing a degree but not complete directional solidification.

The results of stress rupture tests on the directionally solidified castings are plotted in Figure 19, along with the modified and exploratory alloy of this Co - 15 W base alloy. The stress for a 100-hour life at 1850 F increased from 16,000 psi to 19,000 psi compared to the conventionally cast modified alloy; the stress rupture life at 1850 F and 17,500 psi for the directionally solidified alloy increased to 200 hours. The stress rupture life of the alloy based on the time to fracture at an initial stress of 17,500 psi was improved by a factor of 4.2. Partial directional solidification had increased the properties of the alloy to a level comparable with commercial Ni-base alloys such as IN-100 and MAR M 200 (49). This improvement in stress rupture properties between

conventional and directionally solidified castings was rechecked with another set of heats. Stress rupture tests on this second set of castings were in good agreement with the results from the first set of castings.

The data in Table IX indicates that a reduction in precipitate size, mean free path, and secondary dendrite arm spacing occurred with the directional casting. The observed improvement in stress rupture life may be entirely from the refinement of these microstructural features or also the result of the orientation of the precipitates or directionality of the grains with respect to the applied stress.

Since the directional casting involved the use of a chill block, its macrostructure was patently different from that of the conventional casting. The macrostructures of these two castings are exemplified by Figures 17-a and 17-d. In the conventional casting, the grains are relatively large and of a uniform size throughout the gage length. In the directional casting, the grain size varies from extremely fine at the chill end of the gage length to a size approximating that of the conventional casting near the riser. The variation in grain size in the directional casting is accompanied by a less marked variation in precipitate size. To accomodate these variations, the microstructural characteristics were obtained from as near the

middle of the gage length as was possible and thus served as average characteristics for the casting. Except for these variations in size, the microstructures of the conventional and directional castings appeared to be identical.

It is well known that fine-grained materials exhibit lower creep strength at elevated temperatures than do the same materials with a coarse-grained structure (3). The opposite behaviour of the fine-grained materials was observed in this investigation. Further, the test bars rarely fractured at the fine grained end but almost invariably broke near the center of the gage length in both conventionally and directionally cast test bars.

Static oxidation tests on the two castings were made for 71 hours at 1850 F in still air. Even under very slow furnace cooling, the oxide scales of the oxidation samples spalled off completely. As Table X indicates, the conventional casting lost 155.8 mg per square centimeter of original surface area while the directional casting lost 157.4 mg/sq cm. The difference in oxidation resistance is small and slightly inferior for the directional casting, so oxidation resistance could not account for the improved properties of the directional casting.

Examination for microporosity, microshrinkage and inclusions other than discrete precipitates was made but

could not be used to rationalize the difference in properties. Inclusions were not observed in either casting apparently because of the high purity charge materials, inert gas melting and casting atmosphere, and very little attack on the stabilized zirconia crucibles and investment molds. Precipitates which broke during grinding had a tendency to be gouged out and form enlarged cavities during subsequent polishing, making microscopic examination for microporosity or microshrinkage unreliable. Actual density measurements on the test bars showed a density of 0.3382 lbs/cubic inch for the conventional casting and 0.3388 lbs/cubic inch for the directional casting. These figures do not offer any appreciable indication of a microporosity difference between the two types of castings and fail to explain the difference in properties.

The presence of visible surface imperfections, such as pin holes, on the gage length were noted prior to testing the test bars. After testing, the location of the fracture surface was noted in relation to these surface imperfections. After several such observations, it was concluded that these imperfections had no relation with the location of the final fracture surface. At any case, pinholes occurred in the directional castings in about the same frequency as in the conventional castings. Hence, these surface imperfections could not be held as a great

factor in determining the strengths of the castings.

A closer microprobe examination of the two castings indicated that the distribution of elements in the directional casting was practically the same as that in the conventional casting. The only difference between the two was the apparent absence of segregated high chromium areas in the chromium x-ray image of the directional casting. Static probe analysis of the matrix, listed on Table VIII, indicated that the matrix became enriched with Cr and W. The rapid solidification apparently suppressed the formation of the Cr-rich carbides leaving more Cr and W in solution and further strengthening in the matrix. The increase in the concentrations of these elements are not large but their combined effects with the refinement and directionality of microstructural features probably account for the improvement in properties of the directional casting.

Effect of Increased Alloying Additions

Since chromium is recognized as the element primarily responsible for the oxidation resistance of these alloys as indicated by its effect on the oxidation of Co - Cr binary alloys in Figure 23 (50), a higher Cr content of 20 to 30 w/o could be expected to improve the oxidation resistance of these alloys compared to that of the 10 w/o Cr alloy. The preceding discussions have

indicated that Cr was also partly responsible for the strengthening of the alloy through solid solution strengthening of the matrix. The directional solidification process suppressed the formation of Cr-rich carbides thereby increasing the Cr available for matrix strengthening. Accordingly, the addition of more Cr would be expected to further improve strength. The influence of Cr on strength and oxidation resistance was determined by adding up to 20 w/o Cr to the alloy and comparing the results with a control alloy of 10 w/o Cr, 2 w/o Zr, 2 w/o Ti and 1 w/o C.

To minimize the interfering effects of new phases on the evaluation of results it was desirable to keep the matrix single-phased. The Co - W - Cr ternary phase diagram at room temperature shown in Figure 24 (51) indicates that it is possible to increase Cr contents up to about 25 w/o without forming a second phase of the ternary alloy. At higher temperatures, a higher solubility is anticipated. Because the effects of complex additions of alloying elements on the solubility and solidification characteristics of the alloy could not be predicted with great certainty, it was decided to increase the Cr content up to 20 w/o only. Thus, two other sets of directional and conventional castings with Cr contents of 15 w/o and 20 w/o were made. Figure 25 shows that the microstructures of these alloys remained similar to that of the control 10 w/o Cr alloy.

The results of stress rupture tests on these castings are summarized and compared with those of the control and commercial alloys in Figure 26. It is apparent that increasing Cr contents yielded imcreasing elevated temperature properties whether the alloy was cast conventionally or directionally. For a life of 100 hours, the stresses required to rupture the conventionally cast 15 w/o and 20 w/o Cr alloys were 17,000 psi and 18,500 psi respectively, compared to 16,500 psi for the 10 w/o Cr alloy. These correspond to improvements by factors of 1.06 and 1.15 over the control alloy. Likewise, at 17,500 psi and 1850 F, the stress rupture life of the conventional castings increased to 87 hours and 150 hours for the 15 w/o and 20 w/o Cr alloys, respectively. These represent improvements by factors of 1.85 and 3.2 over the stress rupture life of 47 hours of the control alloy.

As previously mentioned, directional solidification improved the properties of the control alloy to a level comparable to those of commercial Ni-base alloys. When directional solidification was applied to the high Cr alloys, the expected improvements were also realized. Their stress rupture lives indicated these to be better than the commercial Ni-base alloys IN 100 and MAR M 200. At 25,000 psi and 1850 F, the directionally cast 20 w/o Cr alloy had a stress rupture life of 28 hours; at

15,000 psi, its stress rupture life was 1,110 hours. These stress rupture properties are intermediate between those of the better commercial Ni-base superalloys and the best experimental Ni-base superalloy available today, the TRW VI-A alloy. This latter TRW alloy had a stress rupture life of 1,600 hours at 15,000 psi and 1850 F (6). With a density of only 0.334 lbs/cubic inch, these alloys also have good properties on a strength-to-density basis, as may be seen from Figure 27.

A common complaint with most Co-base alloys is the cracking or spalling of the oxide scales during cooling from high temperatures. In the static oxidation tests, the oxide scale of the control alloy spalled off completely and necessitated expressing their oxidation rates in terms of weight loss per unit of original surface area. In order to compare its oxidation resistance directly with the others, the results of the shorter continuous weight gain tests were extrapolated. The extrapolation showed a weight gain of about 30 mg/square centimeter of original surface area in 70 hours. Comparing it with the static oxidation test results in Table X shows that the improvement in oxidation resistance is practically proportional to the increase in Cr content and that the scaling behaviour improves with increasing Cr content. At 10 w/o Cr, the scale was rather thick and spalled off

completely during cooling; at 15 w/o Cr, the scale was thinner and more adherent so that only a small fraction spalled off; at 20 w/o Cr, the scale was very thin and completely adherent so that after 71 hours, its gain in weight was only 7.69 mg/sq cm. This improvement in oxidation resistance is reflected in the continued improvement in stress rupture life with increasing Cr contents. It is probable that both strength and oxidation resistance can be improved further by further addition of Cr. The optimum Cr content was not determined in this study and is suggested as a possible object of a future study.

For dispersion hardened materials, it has been shown that the volume fraction of the phase is an important variable (45). With the Zr and Ti contents fixed at 2 w/o each, the volume percent of carbide precipitates in all the alloys remained at about 7 %. An attempt to increase precipitation was made by increasing the Zr and Ti contents to 3 w/o each. The carbon content was also increased to 1.5 w/o in order to keep the (Zr + Ti)/C ratio at 0.76 which, according to Ramseyer (27), was an optimum value. These additions were made on 10 w/o and 15 w/o Cr alloys. Table IX shows that the volume of precipitates indeed increased to about 11 %. However, as Figure 28 shows, this increase took the form of increase in precipitate size rather than increase in number of precipitates.

Figure 29 shows no increase in properties in either the directional or conventional castings.

Since the larger precipitates were Ti-rich, another alloy, where only Zr was raised to 3 w/o, was directionally cast. As shown in Figure 28-b no overly large precipitates formed. Figure 29 shows that this higher zirconium alloy exhibited poor stress rupture behaviour. Apparently, the beneficial effect of Ti, Zr and C additions is not dependent upon the (Zr + Ti)/C ratio alone but also upon the Ti/Zr ratio and the amounts of each element added. This was not clarified in this study but is suggested as a possible object of a future study.

Effect of Casting Conditions:

For any established composition, the casting condition or more specifically, the rate of solidification, was varied to control the precipitate size. This was varied by employing a chill block or varying the mold temperature. All the directional castings discussed previously were produced with a mold temperature of 1600 F. To determine to what extent the precipitates could be refined by this technique and its concommitant effects on the stress rupture properties, three other directional castings were made at mold temperatures of

80 F (unheated mold), 1,000 F and 2320 F for the 15 w/o Cr alloy.

The resulting microstructures are shown in Figure 30; and stress rupture test results in Figure 31. Comparing the castings produced in the molds at 1000 F with the standard 1600 F mold previously discussed, the stress rupture life at 1850 F and 17,500 psi is increased by a factor of almost 2 or from 300 hours to 540 hours. This casting had a secondary dendrite arm spacing of 13.4 microns and about 66 precipitates per lineal millimeter. The casting from the unheated mold had finer precipitates and smaller secondary dendrite arm spacing than the casting from the 1000 F mold but, as shown in Figure 31, did not produce any better stress rupture properties than the casting produced in a mold at 1600 F. This failure to provide improvement is probably the result of discontinuities in the cast stress rupture bars resulting from the rapid solidification and cooling in the cold mold. Contraction stresses produced by resistance of the cold, rigid mold were large enough to cause metal unsoundness at the hotter end of the casting. The casting design with the smaller diameter gage length between the two larger diameter tapered grip sections is susceptible to hot tearing at the junction of the gage

and grip sections of the test bar. The metal unsoundness at this location resulted in hot tears in 2 of the 6 test bars in the cluster casting. The other 4 test bars were sound in external appearance but fractured at or near this location during stress rupture testing.

While these castings produced with the 1000 F and 1600 F molds are termed directionally solidified because of the chill at one end, these test bar castings do not exhibit the usual long columnar grains found in completely directionally solidified castings. This type of grain could only be obtained when the temperature at the top of the mold is maintained close to the melting point of the alloy and the thermal gradient from the top to the bottom of the mold is steep. These conditions did not exist along the entire length of these castings and were not desired because a slower solidification rate would have resulted.

It was decided to study the influence of a completely directionally solidified test bar on the properties. The elongated grain structure of directional solidification was obtained by casting at a mold temperature of 2320 F. The macrostructure of the resulting casting is show in Figure 17-e and does contain elongated grains along the gage length. This type of grain structure

was accompanied by marked segregation of precipitates into interdendritic zones, however, as illustrated in Figure 30-d. With this structure, wide regions of precipitate-free matrix were aligned in the direction of stress application. When the casting was loaded, the precipitate-free region yielded at relatively low stress producing a large elongation of 17% and necking and the low stress rupture life of the casting shown in Figure 31. This result indicates that the strength of the alloy was not obtained simply by solid solution strengthening effects on the matrix but required the presence of the finely divided carbide precipitates randomly distributed in the matrix.

Room Temperature Tensile Properties of the Co - 15 W Base Alloys

The room temperature properties are of some significance because brittle behaviour of these superalloys could produce problems in service. For this reason, the room temperature tensile properties were determined. The results,as shown in Table XI for both the conventionally and directionally cast Co - 15 W base alloys, indicate appreciable strength but poor ductility. This table includes the modified alloys with the better stress rupture properties. The ductility is reported as reduction

in area because the brittleness of the material made it very difficult to obtain accurate measurement of elongation.

The data in Table XI indicates that the room temperature tensile strength improved slightly with higher chromium contents. The tensile strength increased from 98,800 to 112,000 and then to 125,000 psi as the chromium content was raised from 10 to 15 and 20 w/o respectively. The improvement in strength was not accompanied by any significant change in ductility. It is pointed out that the technique employed in this study for optimizing stress rupture strength would not be expected to provide high ductility.

SUMMARY

Various types of congruently melting phases were modified with elements to: (a) enhance oxidation resistance; (b) provide solid solution strengthening; and (c) produce discrete precipitate dispersions from the melt. For oxidation resistance, Cr, Al and Si were used; Zr, Ti, C and B were selected to provide carbides and borides; and for solid solution strengthening, elements with high solid solubility in the binary elements (preferably refractory metals) were selected. All the elements were added at the same time thereby producing complex alloys. Based on stress rupture properties, the promising high temperature alloys were the Fe - 50 Co base alloy and the Co - 15 W base alloy.

In the Fe - 50 Co base alloy, overly large precipitates appeared to produce eventual rupture of the alloy during stress rupture testing. In the Co - 15 W alloy, a eutectic structure caused embrittlement. A microprobe study of the alloys resulted in the following determinations:

(1) Molybdenum and boron produced the eutectic structure in the Co - 15 W base alloy.

(2) Titanium, zirconium, and carbon caused the discrete carbide precipitates in both alloys.

(3) All large precipitates in both alloys were Ti-rich.

(4) Chromium and silicon acted similarly and appeared to have no significant roles as carbide strengtheners but were solid solution strengtheners in both alloys.

These results from the microprobe led to the following changes in composition:

(1) Titanium was decreased in the Fe - 50 Co base alloy to reduce the size of the large precipitates.

(2) Chromium was increased in both alloys to produce improved oxidation resistance and solid solution strengthening. Silicon was eliminated because it simply duplicated the action of chromium.

(3) Molybdenum and boron were removed from the Co - 15 W base alloy to eliminate the deleterious eutectic structure.

The modifications on the alloy composition were successful for the most part in producing the desired changes. Reduction of titanium content eliminated the large precipitates in the Fe - 50 Co base alloy but the stress rupture properties were not improved. The removal of molybdenum and boron from the Co - 15 W base alloy eliminated the eutectic structure, refined the size of the discrete carbide precipitates and greatly improved

its properties to a level comparable with commercial Co-base superalloys. However, the oxidized scale was thick and spalled off completely on cooling from a high temperature. By increasing the Cr content to 20 w/o, the scale became very thin and completely adherent. The stress rupture behaviour also improved to make it comparable to commercial Ni-base superalloys.

Directional solidification was very effective in providing further improvement in the stress rupture behaviour of the alloys. When directionally cast with a mold temperature of 1600 F, the Co - 15 W, 20 Cr, 2 Zr, 2 Ti, 1 C alloy exhibited a stress rupture life at 15,000 psi and 1850 F almost comparable with the TRW VI-A alloy, the best experimental Ni-base alloy. Directional castings poured into molds at lower temperatures had better stress rupture properties but the difficulties of producing sound castings limited the lowest practicable investment mold temperature. Castings with elongated grain structures, promoted by higher mold temperatures, showed segregation of precipitates to interdendritic regions rather than the uniform distribution and produced poor stress rupture strength.

REFERENCES

1. J. E. Campbell, H. B. Goodwin, H. J. Wagner, R. W. Douglass, and B. C. Allen, "Introduction to Metals for Elevated-Temperature Use," DMIC Report 160 (Oct. 27, 1961).

2. G. T. Harris and H. C. Child, "Development of a High-Temperature Alloy for Gas Turbine Rotor Blades," Iron and Steel Institute Special Report No. 43, (July 1952), 67.

3. E. R. Parker, "The Role of Refractory Metals in Superalloys," Proceedings, ASTM, 60 (1960), 849-66.

4. S. T. Scheirer and R. J. Quigg, "Development of High Temperature Nickel-Base Alloys for Jet Engine Bucket Applications," NASA CR-54504, (Oct. 20, 1965).

5. C. T. Sims, "A Contemporary View of Nickel-Base Superalloys," Journal of Metals, (Oct. 1966), 119-30.

6. H. E. Collins, "Development of High Temperature Nickel-Base Alloys for Jet Engine Turbine Bucket Applications," NASA CR-54507, (June 20, 1967).

7. R. Irmann, "Sintered Aluminum with High Strength at Elevated Temperature," Metallurgia, 46 (1952), 125.

8. R. E. Stuart and C. D. Starr, "TD Nickel," Materials in Design Engineering, 58 (August 1963), 81-85.

9. J. G. Rasmussen and N. J. Grant, "ThO_2-Dispersion Hardened Nickel and Nickel-Molybdenum Alloys Produced by Selective Reduction," Powder Metallurgy, 8 (1965), 92-112.

10. D. A. Roberts, "Review of Recent Developments in the Technology of Nickel-Base and Cobalt-Base Alloys," DMIC Memorandum 135, (Oct. 31, 1961).

11. R. F. Cheney and J. S. Smith, "Development of Dispersion-Strengthened Nickel- and Cobalt-Base Alloys," Yearly Summary Report, Sylvania Electric Products, Inc., Contract AF 33(615)-1697, (Aug. 31, 1965).

12. L. F. Norris, B. W. Kushnir and R. W. Fraser, "Improvement of the Properties of Dispersion Strengthened Nickel-Chromium Alloys," Final Report AFML-TR-68-67, Sherritt Gordon Mines Limited, Contract AF 33(615)-3208, (March 1968).

13. E. F. Adkins, C. T. Sims and R. I. Jaffee, "Nonmetallic dispersions in Cobalt," Trans. Met. Soc. AIME, 215 (April 1959), 344-52.

14. A. L. Mincher and D. B. Arnold, "Development of Dispersion Strengthened Cobalt-Base Alloys," Final Report AFML-TR-68-95, E. I. du Pont de Nemours & Co., Inc., (April 1968).

15. O. Preston and N. J. Grant, "Dispersion Strengthening of Copper by Internal Oxidation," Trans. Met. Soc. AIME, 221 (February 1961), 164-73.

16. L. J. Bonis and N. J. Grant, "The Structure and Properties of Dispersion Strengthened Internally Oxisized Nickel Alloys," Trans. Met. Soc. AIME, 224 (April 1962), 308-16.

17. W. M. Schwarzkopf and N. J. Grant, "Fine Particle Strengthening for High Temperature Use," in Proceedings, Third Plansee Seminar, (June 22-26, 1958), 454-64.

18. M. Yamazaki and N. J. Grant, "Alumina Dispersion-Strengthened Copper-Nickel Alloys," Trans. Met. Soc. AIME, 233 (Aug. 1965), 1573-80.

19. J. S. Wolf, J. W. Weeton and J. C. Freche, "Observations of Internal Oxidation in Six Nickel-Base Alloy Systems," NASA Report TN D-2813, (May 1965).

20. N. J. Grant, "Dispersion Strengthening," in Strengthening Mechanisms: Metals and Ceramics, Proceedings, 12th Sagamore Army Materials Research Conference, Syracuse University Press, (1966), 63-82.

21. R. I. Jaffee and G. T. Hahn, "Structural Considerations in Developing Refractory Metal Alloys," DMIC Report 182, (Jan. 31, 1963).

22. W. S. Cremens, "Use of Submicron Metal and Nonmetal Powders for Dispersion-Strengthened Alloys," in Ultrafine Particles, edited by W. E. Kuhn, H. Lamprey and C. Sheer, John Wiley & Sons, Inc., New York, (1963), 457-78.

23. M. Gensamer, E. G. Pearsall, W. S. Pellini and J. R. Low Jr., "The Tensile Properties of Pearlite, Bainite and Spheroidite," Trans. ASM, 30 (1942), 983-1020.

24. N. E. Ryan and S. T. M. Johnstone, "Alloys of Chromium, Titanium, and Nitrogen," J. Less Common Metals, 8 (1965), 159-64.

25. R. L. Ashbrook and J. F. Wallace, "Modification of Eutectic Alloys for High Temperature Service," Trans. Met. Soc. AIME, 236 (1966), 670-78.

26. S. F. Ramseyer and J. F. Wallace, "Modified Eutectic Alloys for High Temperature Service," Second Year Interim Report on NASA Grant SC-NsG 639/36-033-033, Case Institute of Technology, (June 1966).

27. S. F. Ramseyer, "Control of Cast Structures of Alloys for High Temperature Service," Ph.D. Thesis, Case Institute of Technology, (November 1966).

28. Z. Jeffries, "Aluminum-Silicon Alloys," Chemical and Metallurgical Engineering, 26 (April 19, 1922), 750.

29. R. C. Plumb and J. E. Lewis, "The Modification of Aluminum-Silicon Alloys by Sodium," J. Inst. Metals, 86 (1957-58), 393-400.

30. F. L. VerSnyder, R. B. Barlow, L. W. Sink and B. J. Piearcey, "Directional Solidification in the Precision Casting of Gas Turbine Parts," Trans. AFS, 75 (1967), 360-67.

31. N. J. Grant, "The Influence of Metal Structure on Properties of Investment Castings, Part I," Precision Metal Molding, 12 (Sept. 1954), 122-26.

32. B. J. Piearcey and F. L. VerSnyder, "A New Development in Gas Turbine Materials--The Properties and Characteristics of PWA 664," AIAA Paper No. 65-742, (Nov. 1965).

33. B. J. Piearcey and F. L. VerSnyder, "A Breakthrough in Making Turbine Components . . . Directional Solidification and Single Crystals," Metal Progress, 90 (Nov. 1966), 66-71.

34. F. L. VerSnyder and B. J. Piearcey, "Single Crystal Alloy Extends Turbine Blade Service Life to Four Times," SAE Journal, 74 (Aug. 1966), 36.

35. F. L. VerSnyder and R. W. Guard, "Directional Grain Structures for High Temperature Strength," Trans. ASM, 52 (1960), 485-93.

36 C. Vishnevsky, "Structural Effects on Stress Rupture and Superplasticity Behaviour in Co - W Alloys," Ph.D. Thesis, Case Institute of Technology, (Nov 1967).

37. B. Chalmers, Principles of Solidification, John Wiley & Sons, Inc., New York, (1964), 206-19.

38. H. E. Collins, R. J. Quigg and R. L. Dreshfield, "Development of a Nickel Base Superalloy Using Statistically Designed Experiments," Trans, ASM, 61 (1968), 711-21.

39. "Moly Pays Off," Climax Molybdenum Corp., 2 (March 1969), 2.

40. M. Hansen and K. Anderko, Constitution of Binary Alloys, McGraw-Hill Book Co., New York, (1958).

41. E. E. Underwood, Quantitative Metallography," Metals Engineering Quarterly, 1 (1961), Part 1: No. 3, pp, 70-80, Part 2: No. 4, pp. 62-70

42. J. N. Goodier, "Concentration of Stress Around Spherical and Cylindrical Inclusions and Flaws," J. Applied Mechanics, 1 (1933), 39-44.

43. F. Garofalo, Fundamentals of Creep and Creep-Rupture in Metals, The Macmillan Co., New York, (1965).

44. W. S. Cremens and N. J. Grant, "Preparation and High Temperature Properties of Nickel-Al_2O_3 Alloys," Proceedings, ASTM, 58 (1958), 714-32.

45. N. J. Grant, "Dispersed Phase Strengthening," in The Strengthening of Metals, edited by D. Peckner, Reinhold Publishing Corp., New York, (1964), 163-99.

46. R. W. Guard, "Mechanisms of Fine Particle Strengthening," in Strengthening Mechanisms in Solids, ASM,

47. H. J. Wagner and A. M. Hall, "The Physical Metallurgy of Cobalt-Base Superalloys," DMIC Report 171, (July 6, 1962).

48. J. C. Freche, R. L. Ashbrook and G. D. Sandrock, "The Potential for Cobalt-Tungsten Superalloys," Metal Progress, 87 (May 1965), 74-79.

49. J. C. Freche and W. J. Waters, "High Temperature Service Offered by New Nickel-Base Alloys," Foundry, 92 (July 1964), 44-47.

50. C. A. Phalnikar, "The Scaling of Cobalt-Chromium Alloys in Air," Ph.D. Thesis, Case Institute of Technology, (July 1952).

51. J. J. English, "Binary and Ternary Phase Diagrams of Columbium, Molybdenum, Tantalum, and Tungsten," DMIC Report 183, (Feb. 7, 1963).

52. H. L. Wheaton, "MAR M 509, A new Cobalt-Base Alloy for High Temperature Service," Cobalt, 29 (Dec. 1965), 163-70.

TABLE I

COMPOSITION OF EXPLORATORY BINARY ALLOYS

Alloy Composition w/o	Melting Point deg C	Crystal Structure	Maximum Solubility w/o
Cr - 20 Mo	1860	BCC	100
Fe - 65 Ni	1436	FCC > 250	100
Fe - 22 Cr	1507	BCC	100
Ti - 30 V	1620	BCC	100
Co - 15 W	(1500)	FCC > 800	37% W
Fe - 34 Mo	1450	FCC > 1425 FCC + ϵ < 1425	37.5% Mo
Fe - 50 Co	1480	FCC > 980 BCC > 730 ordered BCC < 730	100
Ti - 47 Cr	1390	BCC > 1300 BCC + $TiCr_2$ > 675 HCP + $TiCr_2$ < 675	100
Mn - 10 Fe	1240	FCC > 1140 cubic < 1130	100
Fe - 30 Ti	(1427)	$TiFe_2$	
Fe - 45 Cb	(1655)	$CbFe_2$	
Cr - 15 Si	(1730)	Cr_3Si	

Note: Alloys with melting points in parenthesis are maximum-melting-point type alloys.

TABLE II

PROPERTIES OF ELEMENTS USED (53)

Element	Crystal Structure at degrees C	Goldschmidt Atomic Radius Angstrom	Melting Point degrees C
Al	FCC	1.43	660
B	--	0.92	2100 to 2200
C	--	0.77	--
Cb	BCC	1.47	2468
Co	HCP < 400 C	1.25	1495
Cr	BCC	1.28	1875
Fe	BCC < 910 FCC > 910 BCC > 1390	1.27	1534
Mn	cubic < 1095 BCC > 1133	1.30	1234
Mo	BCC	1.40	2620
Ni	FCC	1.25	1452
Si	cubic	1.34	1412
Ti	HCP < 880 BCC > 880	1.47	1670
V	BCC	1.36	1900
W	BCC	1.41	3380
Zr	HCP < 865 BCC > 865	1.60	1852

TABLE III - MELTING STOCK

Element	Purity %	Form
Boron	99.30	-325 mesh
Carbon	99.999+	Spectroscopic graphite
Cobalt	99.5	Electrolytic, 1"x1"x1/8"
Chromium	99.85+	Electrolytic
Molybdenum	99.9+	-200 mesh
Nickel	99.9	Electrolytic, 1"x1"x1/8"
Titanium	99.65	Sponge
Tungsten	99.9	Powder, 6 micron ave.
Vanadium	99.50	Chips
Zirconium	99.8	Reactor grade sponge
Iron	99.9	Electrolytic, 1"x1"x1/8"
Columbium	99.5	-10 mesh
Silicon	99.65	Chips

TABLE IV

BASIC COMPOSITION AND HARDNESS OF ARC-MELTED BINARY ALLOYS

Binary weight %	Room Temp. Hardness Rc	Remarks
Fe - 30 Ti	18.1	Cracked badly while cooling down. All indentations cracked badly.
Mn - 10 Fe	55.0	All indentations cracked badly.
Fe - 45 Cb	--	Cracked while cooling down. Splintered when load was applied.
Cr - 15 Si	--	Cracked while cooling down. Splintered when load was applied.
Fe - 37.5 Ti	62.10	Two indentations slightly cracked.
Fe - 65 Ni	0	Extremely soft.
Fe - 22 Cr	7.02	
Fe - 50 Co	13.04	
Co - 15 W	22.98	
Ti - 47 Cr	56.78	One indentation slightly cracked.
Fe - 34 Mo	60.00	
Cr - 20 Mo	45.87	Two indentations slightly cracked.

TABLE V

COMPOSITIONS OF EXPLORATORY ALLOYED BINARIES AND RESULTS OF STRESS RUPTURE TESTS

Base Alloy Wt %	Wt % Alloying Elements Added for: Solid Soln: Strength	Dispersed Phases	Oxidation Resistance	1850 F Life at 10 ksi	Remarks
Ti - 30 V	5 Co 2 W 5 Al	2 Zr 1 C 0.5 B	5 Cr	0.09	Many brittle cracks along gage length
Fe - 37.5 Ti	5 Mo	2 Zr 1 C 0.5 B	5 Cr 2 Si	---	All test bars broke while mold was being removed
Ti - 47 Cr	5 Co 5 W 5 Cb	0.2 Zr 0.1 C	---	---	All test bars broke while mold was being removed
Fe - 34 Mo	5 W	2 Zr 2 Ti 1 C 0.5 B	2 Cr 2 Si	1.10	Thick bubbly oxide scale with mottled appearance.
Fe - 34 Mo	---	---	---	1.23	Thick grey oxide scale

TABLE V - Continued

Base Alloy Wt %	Wt % Alloying Elements Added for: Solid Soln: Strength	Dispersed: Phases	Oxidation: Resistance	1850 F Life at 10 ksi	Remarks
Fe - 15 W	5 Co	2 Zr 2 Ti 1 C 0.1 B	5 Cr 2 Si 2 Al	0.13	Elongated as fast as load was applied
Fe - 22 Cr	5 Co 5 W	2 Zr 2 Ti 1 C 0.1 B	2 Si 2 Al	0.15	Elongated as fast as load was applied
Fe - 50 Co	5 W	2 Zr 2 Ti 1 C	5 Cr 2 Si	42.48	Formed greyish scale which spalled off when cooling
Co - 15 W	5 Mo	2 Zr 2 Ti 1 C 0.5 B	5 Cr 2 Si	57.15	Formed shiny oxide scale which spalled off when cooling.

TABLE VI

STATIC PROBE ANALYSES OF PHASES IN THE Fe - 50 Co AND Co - 15 W BASE EXPLORATORY ALLOYS

	Fe w/o	Co w/o	W w/o	Cr w/o	Zr w/o	Ti w/o	C w/o	Si w/o	Mo w/o	B w/o
A. Fe - 50 Co base alloy										
Nominal overall cmpn	41.5	41.5	5	5	2	2	1	2	---	---
Matrix	44.3	40.6	1.4	6.4	0.0	0.4	2.8	---	---	---
Ti-rich precipitate	1.6	1.5	35.3	0.5	3.3	38.5	13.2	---	---	---
Zr-rich precipitate	2.3	4.7	8.1	0.8	68.8	3.4	8.2	---	---	---
B. Co - 15 W base alloy										
Nominal overall cmpn	---	70.1	12.4	5	2	2	1	2	5	0.5
Matrix	---	62.8	3.0	6.3	0.0	0.5	0.6	0.6	1.3	---
Ti-rich precipitate	---	3.7	26.0	0.9	3.3	30.0	9.0	0.0	5.0	---
Zr-rich precipitate	---	8.4	11.6	3.0	41.0	5.8	---	0.0	2.2	---
Eutectic structure	---	77.8	8.6	5.3	0.0	0.8	3.1	0.8	5.0	---
Inner oxide scale	---	39.8	8.5	9.7	0.0	0.7	2.0	1.4	---	---
Outer oxide scale	---	72.4	---	---	---	---	---	---	---	---

TABLE VII

RESULTS OF STRESS RUPTURE TESTS AT 1850 F IN AIR ON THE EXPLORATORY AND MODIFIED ALLOYS

Alloys	Cast Condition	Initial Stress, psi	Time to Fracture, Hours
Fe - 50 Co exploratory	conventional	10,000	52.38
		12,500	15.20
		12,500	2.30
		15,000	0.29
Fe - 50 Co Modified	conventional	10,000	3.79
		15,000	0.25
Fe - 50 Co modified	directional	10,000	20.69
		15,000	0.39
Co - 15 W exploratory	conventional	10,000	57.15
		12,500	11.23
		15,000	4.80
Co - 15 W modified	conventional	15,000	159.36
		17,500	61.95
		20,000	14.19
		20,000	9.31
		25,000	2.15
Co - 15 W modified	directional	15,000	588.63
		20,000	60.41
		20,000	89.52
		25,000	11.90

Note: All castings were made with a mold temperature of 1,600 F.

TABLE VIII

RESULTS OF STATIC PROBE ANALYSES OF PHASES IN THE
Co - 15 W, 10 Cr, 2 Zr, 2 Ti, 1 C ALLOY

	Co w/o	W w/o	Cr w/o	Zr w/o	Ti w/o	C w/o
A. Conventionally cast						
Nominal overall composition	72.75	12.75	10	2	2	1
Matrix	71.2	5.0	11.4	0.0	---	1.9
Ti-rich precipitate	1.9	38.3	1.1	16.8	22.2	5.8
Zr-rich precipitate	2.2	12.5	0.5	47.2	8.5	4.8
Cr-rich precipitate	32.4	7.3	48.6	0.0	0.3	4.3
B. Directionally cast						
Matrix	73.7	5.9	12.5	0.0	0.8	1.8
Ti-rich precipitate	1.9	41.2	0.9	3.4	31.6	10.4

TABLE IX

MICROSTRUCTURAL DATA FROM AS-CAST TEST BARS OF Co - 15 W BASE ALLOYS

Alloying Elements Added w/o	Volume fraction of ppts. %	Secondary dendrite arm spacng microns	No. of ppts per lineal mm	Arithmetic mean ppt size microns	Mean free path microns
A. Conventionally cast					
10 Cr, 2 Zr, 2 Ti, 1 C	6.63	19.1	33.2	3.55	24.95
15 Cr, " " "	6.68	30.1	32.3	3.14	22.45
20 Cr, " " "	7.11	10.1	54.4	2.94	17.09
10 Cr, 3 Zr, 3 Ti, 1.5 C	11.53	24.0	41.36	5.02	21.39
15 Cr, " " "	10.03	21.0	40.0	4.08	22.61
B. Directionally cast					
10 Cr, 2 Zr, 2 Ti, 1 C	7.07	12.3	42.5	3.24	21.8
15 Cr, " " "	7.38	15.8	45.0	2.88	20.6
20 Cr, " " "	7.59	10.0	69.6	2.31	13.20

TABLE IX - Continued

Alloying Elements Added w/o	Volume fraction of ppts. %	Secondary dendrite arm spacng microns	No. of ppts per lineal mm	Arithmetic mean ppt size microns	Mean free path microns
B. Directionally cast - continued					
15 Cr, 3 Zr, 3 Ti, 1.5 C	10.86	---	45.3	2.90	19.66
15 Cr, 3 Zr, 2 Ti, 1 C	7.29	14.2	68.6	2.47	19.25
15 Cr, 2 Zr, 2 Ti, 1 C (a)	7.75	8.3	75.0	1.84	12.30
" " " " (b)	7.88	13.4	66.3	2.19	13.89
" " " " (c)	5.23	28.4	62.11	1.95	15.26

(a) Directionally cast in an unheated mold (80 F).
(b) " " in a mold held at 1,000 F.
(c) " " " " " " " 2.320 F.

TABLE X

RESULTS OF STATIC OXIDATION TESTS ON THE Co - 15 W, 2 Zr, 2 Ti, 1 C BASE ALLOYS FOR 71 HOURS AT 1850 F IN STILL AIR

Chromium content w/o	Casting condition	Wt. change per unit orig. area mg/square cm	Scaling Behaviour
10 Cr	conventional, 1,600 F mold	-155.8	Thick, spalled off completely
15 Cr	"	+ 14.26	Thin, partially adherent
20 Cr	"	+ 7.69	Very thin adherent
10 Cr	directional, 1,600 F mold	-157.4	Spalled off completely
15 Cr	"	+ 17.69	Partially adherent
"	directional, unheated mold	+ 12.93	"
"	directional, 1,000 F mold	+ 13.48	"
"	directional, 2,320 F mold	+ 16.74	"

TABLE XI

ROOM TEMPERATURE PROPERTIES OF THE
Co - 15 W Base Alloys

Alloying elements added w/o	Density lbs/in	Tensile strength psi	Reduction in area %
A. Conventionally cast			
10 Cr, 2 Zr, 2 Ti, 1 C	0.3382	98,800	1.8
15 Cr, " " "(a)	0.3359	112,000	2.2
20 Cr, " " "	0.3338	125,000	1.9
10 Cr, 3 Zr, 3 Ti, 1.5 C	0.3326	99,200	1.50
15 Cr, " " "	0.3251	110,700	1.6
B. Directionally cast			
10 Cr, 2 Zr, 2 Ti, 1 C	0.3388	98,100	2.2
15 Cr, " " "(a)	0.3340	103,300	1.1
15 Cr, 3 Zr, 3 Ti, 1.5C	0.3291	126,500	2.00
15 Cr, 3 Zr, 2 Ti, 1 C(a)	0.3296	110,500	2.50
15 Cr, 2 Zr, 2 Ti, 1 C(a,b)	0.3209	--	--
" " " " (c)	0.3347	117,000	1.00
" " " " (a,d)	0.3330	105,500	1.80

(a) Melting point is approximately 3025 F.
(b) Directionally cast in an unheated mold (80 F).
(c) " " at a mold temperature of 1000 F.
(d) " " " " " " "

TABLE XII

STATIC PROBE ANALYSES OF PHASES IN THE Co - 15 W BASE ALLOYS

	Co w/o	W w/o	Cr w/o	Zr w/o	Ti w/o	C w/o
A Conventionally cast (a)						
15 Cr, 2 Zr, 2 Ti, 1 C,						
Matrix	72.1	5.4	18.1	0.0	0.8	2.1
Ti-Rich precipitate	2.0	35.4	1.3	5.5	19.0	10.1
20 Cr, 2 Zr, 2 Ti, 1 C,						
Matrix	70.4	5.7	19.0	0.0	0.7	----
Ti-rich precipitate	2.2	28.4	5.3	8.5	21.6	----
15 Cr, 3 Zr, 3 Ti, 1.5 C,						
Matrix	76.3	6.2	17.7	0.0	0.8	2.2
Ti-rich precipitate	0.6	36.7	1.8	3.6	29.0	11.4
10 Cr, 3 Zr, 3 Ti, 1.5 C,						
Matrix	76.4	13.6	12.2	0.0	0.9	2.8
Ti-Rich precipitate	2.2	40.3	1.2	4.9	33.8	10.8
B. Directionally cast (b)						
15 Cr, 2 Zr, 2 Ti, 1 C,						
Matrix	64.9	4.3	18.6	0.0	0.7	1.7

TABLE XII - Continued

	Co w/o	W w/o	Cr w/o	Zr w/o	Ti w/o	C w/o
B. Directionally cast-continued						
20 Cr, 2 Zr, 2 Ti, 1 C						
Matrix	64.2	5.3	22.0	0.0	0.7	--
15 Cr, 3 Zr, 3 Ti, 1.5 C,						
Matrix	76.9	4.8	16.3	0.0	0.9	2.2
Ti-rich precipitate	2.1	38.0	1.4	6.2	30.1	12.6
15 Cr, 3 Zr, 2 Ti, 1 C						
Matrix	77.5	6.3	14.2	0.0	0.8	1.4
Zr-Rich precipitate	3.7	13.6	0.9	28.8	3.9	----
15 Cr, 2 Zr, 2 Ti, 1 C (c)						
Matrix	72.3	5.4	18.6	0.0	0.8	2.1
15 Cr, 2 Zr, 2 Ti, 1 C (d)						
Matrix	77.2	7.2	17.6	0.0	0.8	1.4
15 Cr, 2 Zr, 2 Ti, 1 C (e)	70.0	6.1	16.8	0.0	0.8	2.4
Matrix	4.5	35.3	1.9	8.2	27.8	10.8
Ti-Rich precipitate						

TABLE XIII

RESULTS OF STRESS RUPTURE TESTS AT 1850 F IN AIR ON AS-CAST Co - 15 W BASE ALLOYS

Alloying elements added w/o	Initial stress, psi	Time to fracture, hours
A. Conventionally cast alloys		
10 Cr, 2 Zr, 2 Ti, 1 C	15,000	159.36
	17,500	61.95
	20,000	9.31
	20,000	14.19
	25,000	2.15
15 Cr, 2 Zr, 2 Ti, 1 C	15,000	332.12
	17,500	77.20
	20,000	23.88
	25,000	3.41
20 Cr, 2 Zr, 2 Ti, 1 C	15,000	615.22
	17,500	161.84
	20,000	54.50
	25,000	6.52
10 Cr, 3 Zr, 3 Ti, 1.5 C	15,000	176.01
	17,500	37.3
	20,000	21.36
	22,500	3.32
	25,000	1.00
15 Cr, 3 Zr, 3 Ti, 1.5 C	15,000	190.87
	17,500	42.15
	20,000	13.86
	25,000	2.05
B. Directionally cast alloys		
10 Cr, 2 Zr, 2 Ti, 1 C	15,000	588.63
	20,000	60.41
	20,000	89.52
	25,000	9.17
	25,000	11.90

TABLE XIII - Continued

Alloying elements added w/o	Initial Stress, psi	Time to fracture, hours
B. Directionally cast alloys		
15 Cr, 2 Zr, 2 Ti, 1 C	17,500	290.08
	20,000	72.04
	22,500	28.61
	25,000	25.77
20 Cr, 2 Zr, 2 Ti, 1 C	15,000	1109.65
	20,000	93.93
	25,000	28.09
15 Cr, 3 Zr, 3 Ti, 1.5 C	17,500	89.05
	20,000	37.74
	22,500	21.39
	25,000	5.15
15 Cr, 3 Zr, 2 Ti, 1 C	15,000	212.30
	20,000	22.05
	22,500	11.84
	25,000	2.46
15 Cr, 2 Zr, 2 Ti, 1 C(a)	17,500	172.48
	20,000	77.66
	22,500	36.87
	25,000	12.25
15 Cr, 2 Zr, 2 Ti, 1 C(b)	15,000	344.06
	17,500	929.85
	20,000	130.29
	22,500	45.89
	25,000	14.15
15 Cr, 2 Zr, 2 Ti, 1 C(b)	15,000	144.58
	17,500	36,88
	20,000	7.26
	25,000	1.12

(a) Directionally cast in an unheated mold (80F)
(b) " " in a mold held at 1,000 F.
(c) " " " " " " " 2,320 F.

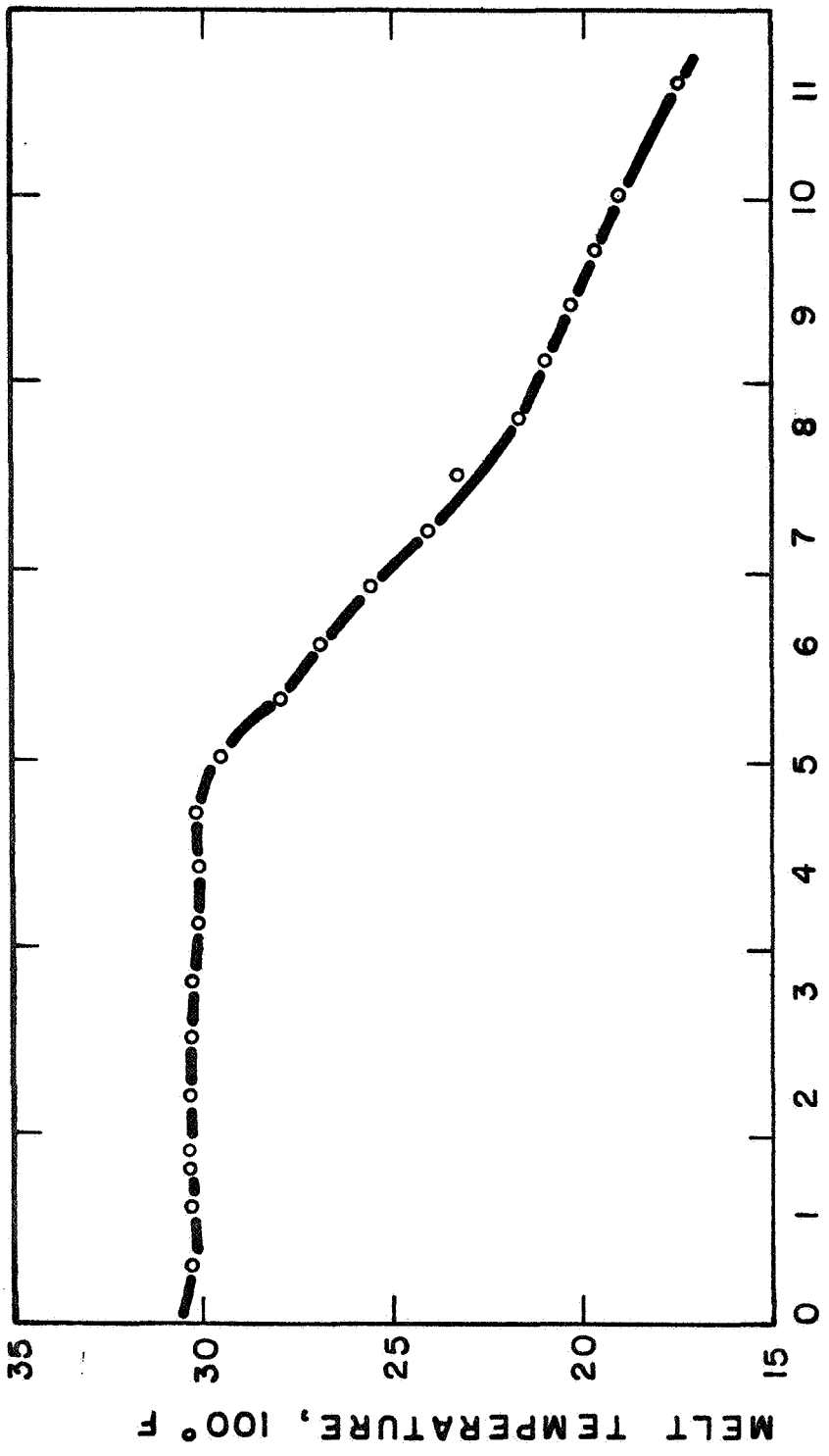

FIGURE I. THERMAL ANALYSIS CURVE FOR THE Co-15W, 15Cr, 2Zr, 2Ti, IC ALLOY.

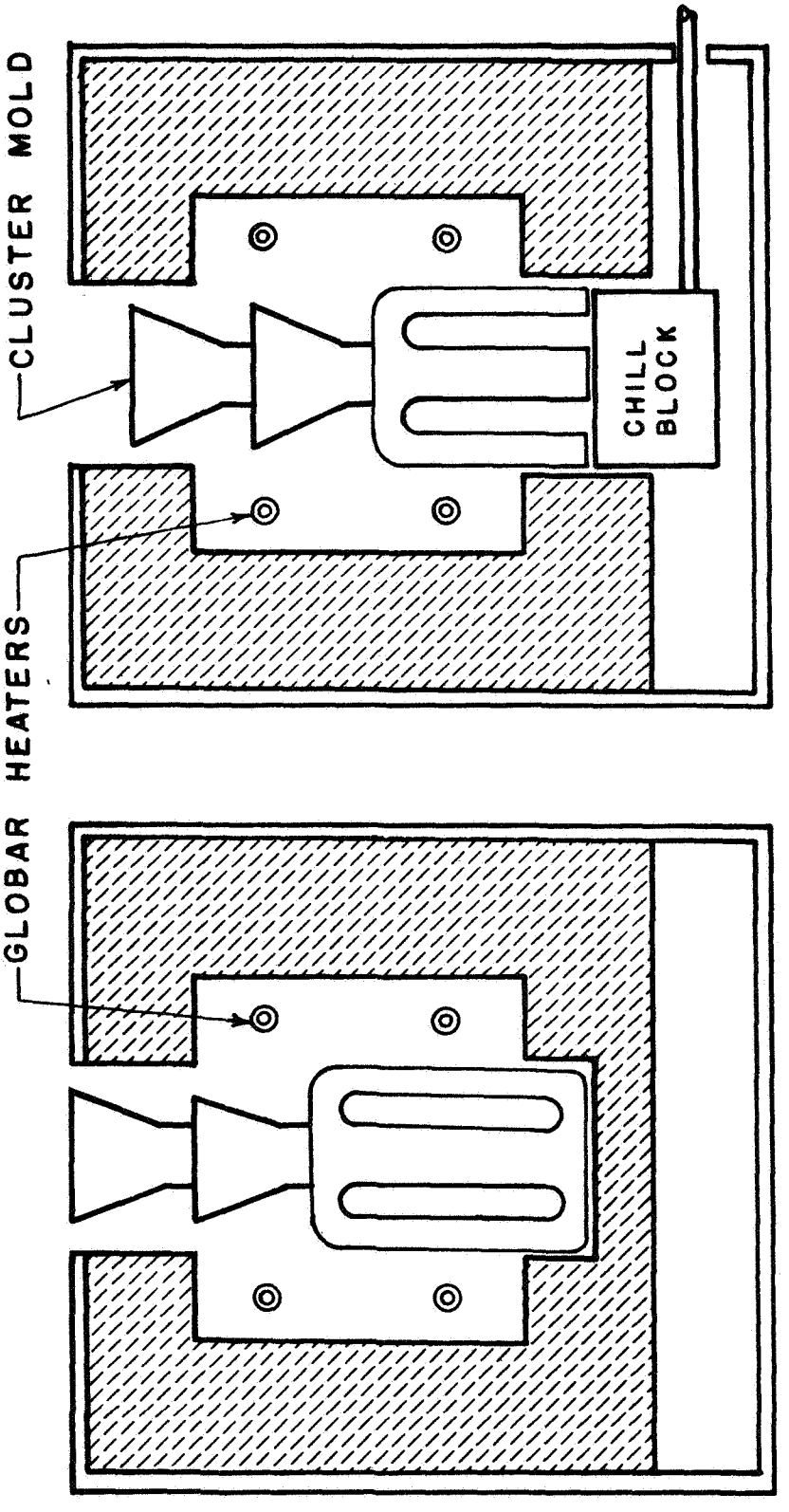

FIG. 2: MOLD FURNACE SET-UP FOR MAKING THE CONVENTIONAL AND DIRECTIONAL CASTINGS.

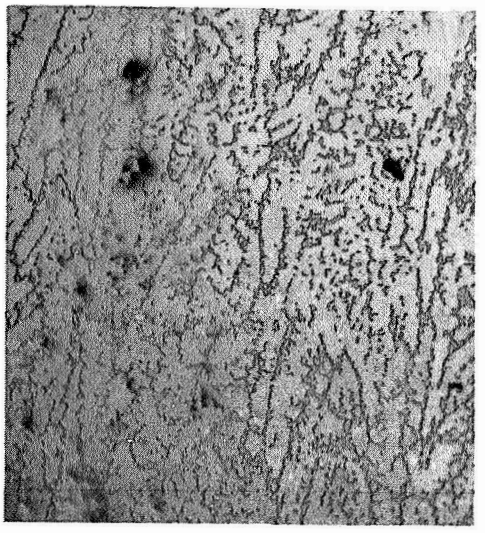

a. Fe - 37.5 Ti X100

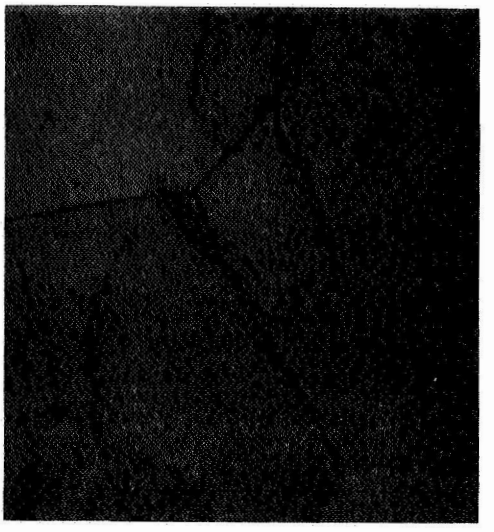

b. Fe - 65 Ni X250

c. Fe - 22 Cr X100

d. Fe - 50 Co X250

Figure 3. Microstructure of chill-cast exploratory binary alloys.

a. Co - 15 W X250

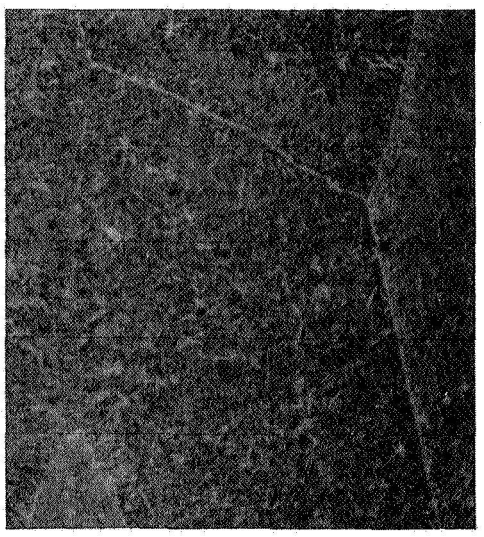

b. Ti - 47 Cr X250

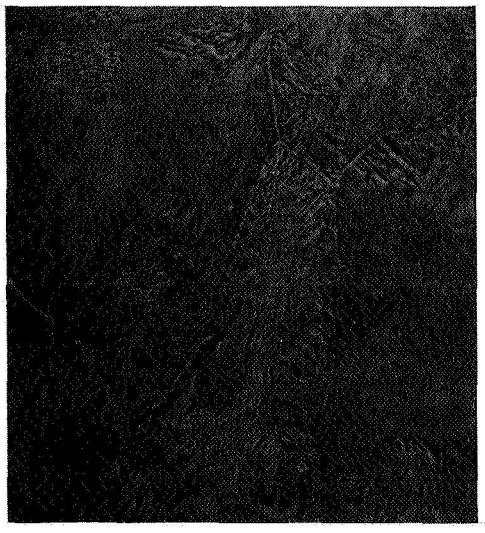

c. Fe - 34 Mo X250

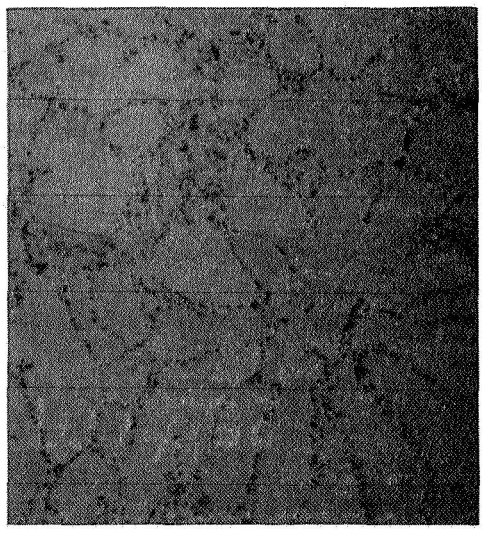

d. Cr - 20 Mo X250

Figure 4. Microstructure of chill-cast binary alloys.

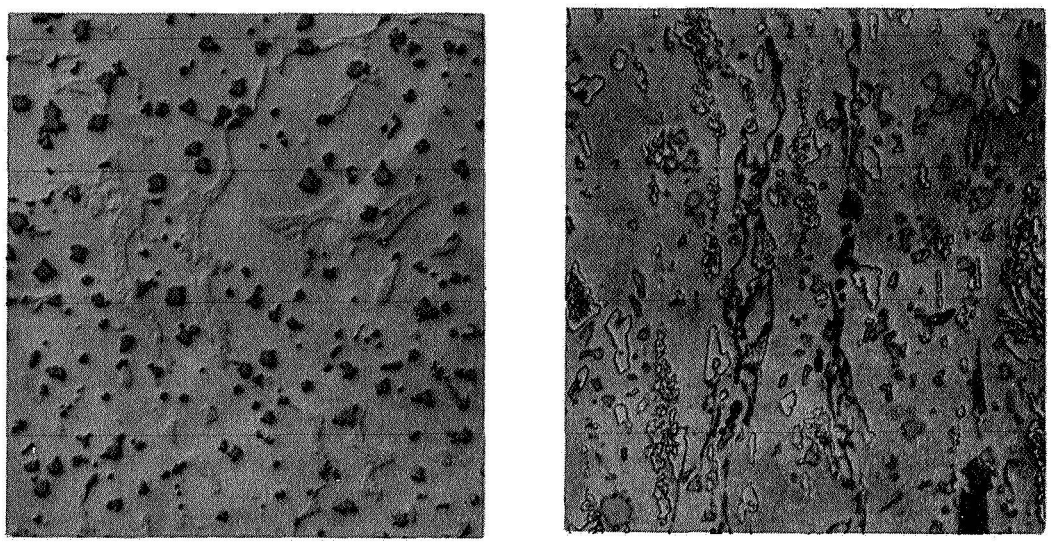

a. Untested b. Tested

Fe - 15 W base alloy

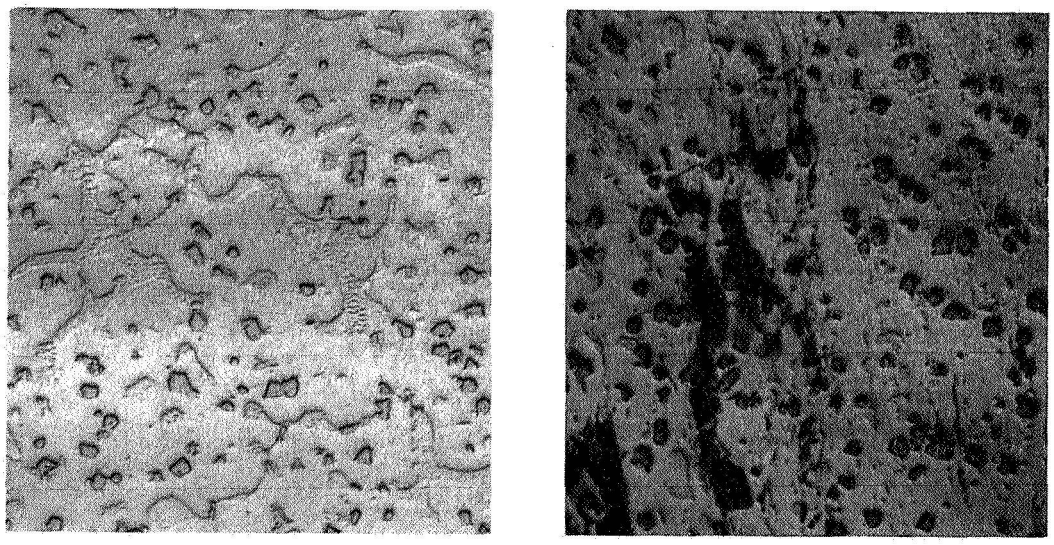

c. Untested d. Tested

Fe - 22 Cr base alloy

Figure 5. Microstructure of exploratory Fe - 15 W and Fe - 22 Cr base alloys. Direction of applied stress is vertical. X250

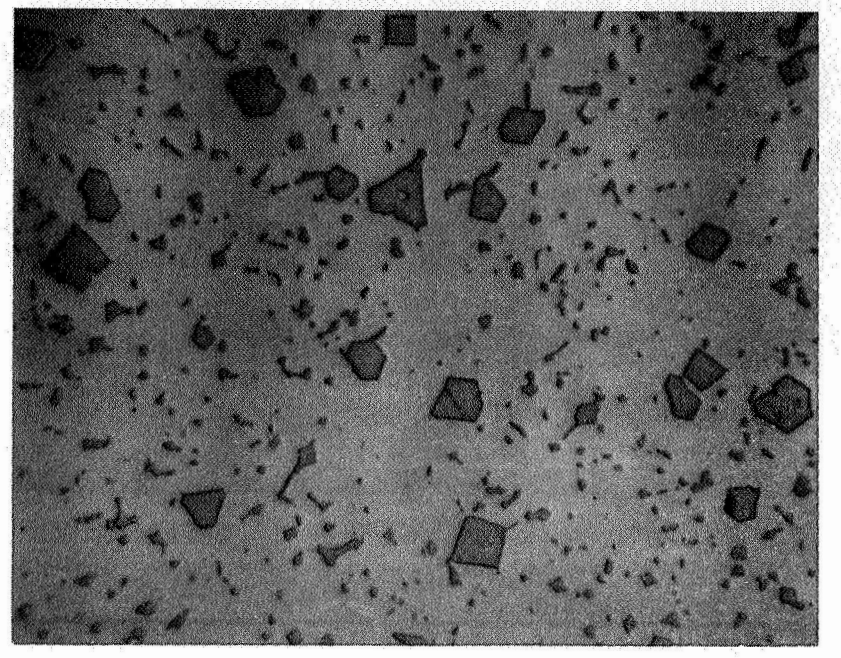

a. Untested

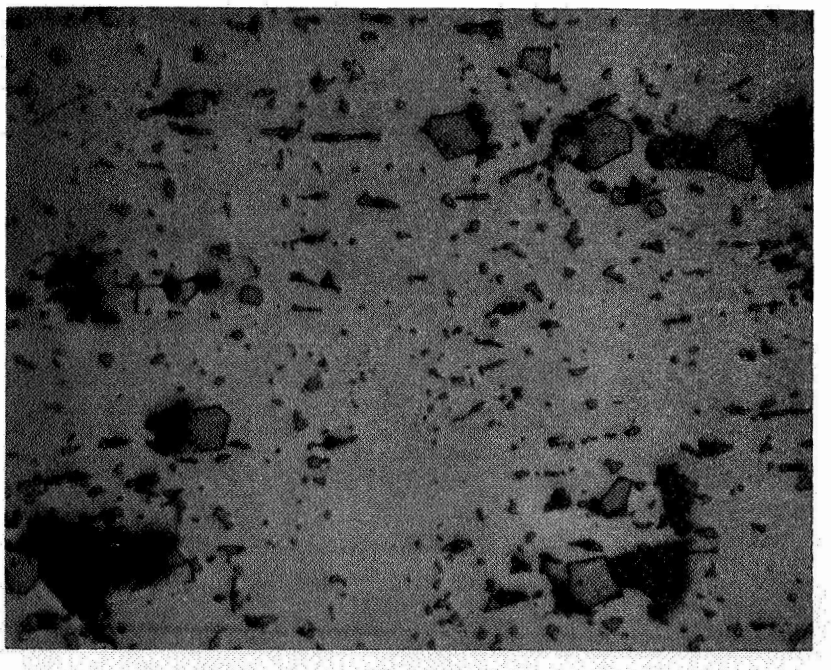

b. Tested

Figure 6. Microstructure of exploratory Fe - 50 Co base alloy. Direction of applied stress is horizontal. X250

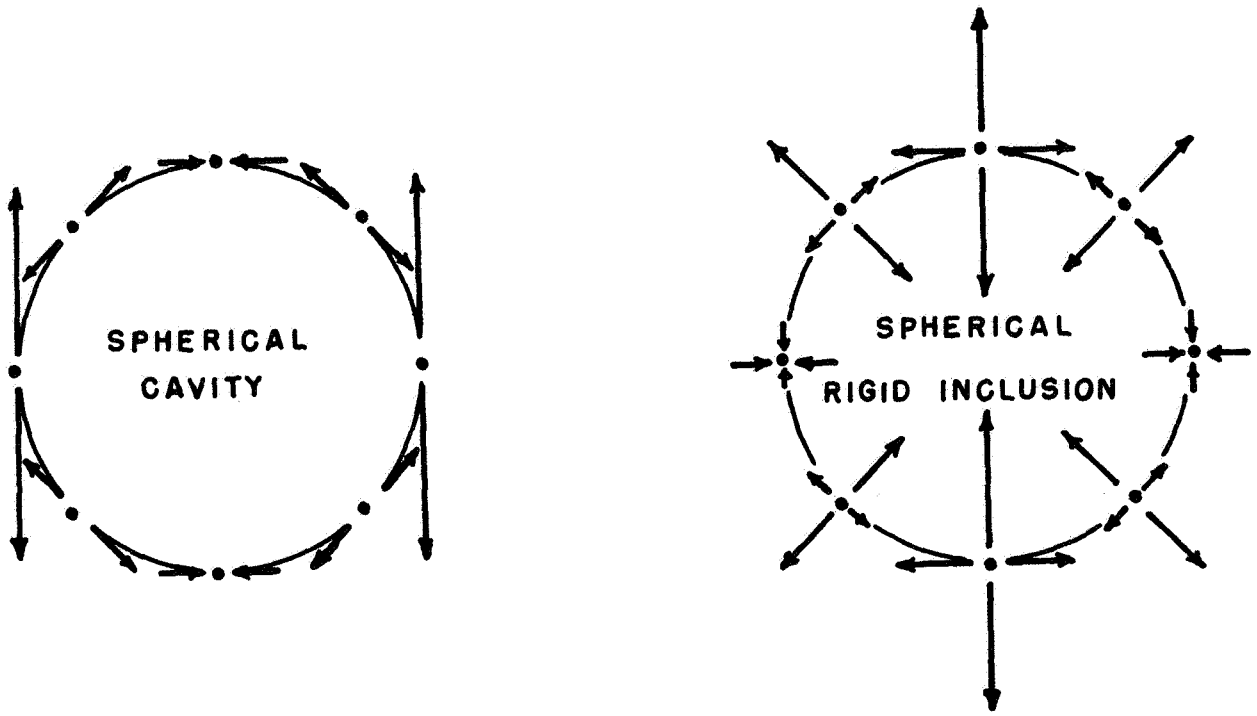

FIGURE 7: INTERFACE STRESSES BETWEEN AN ELASTIC MATRIX AND A SPHERICAL VOID AND A SPHERICAL RIGID INCLUSION (AFTER GOODIER (42)). DIRECTION OF APPLIED STRESS IS VERTICAL.

Figure 8. Microstructure of area examined for the distribution of elements in the exploratory Fe - 50 Co base alloy. X1000

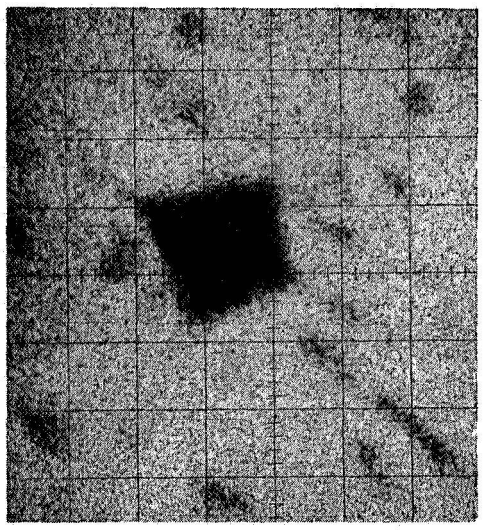

a. Iron

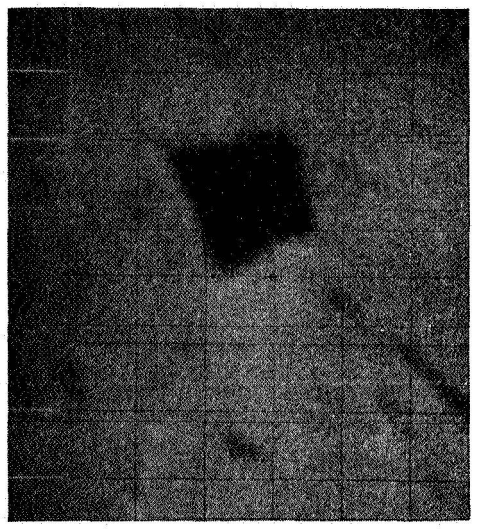

b. Cobalt

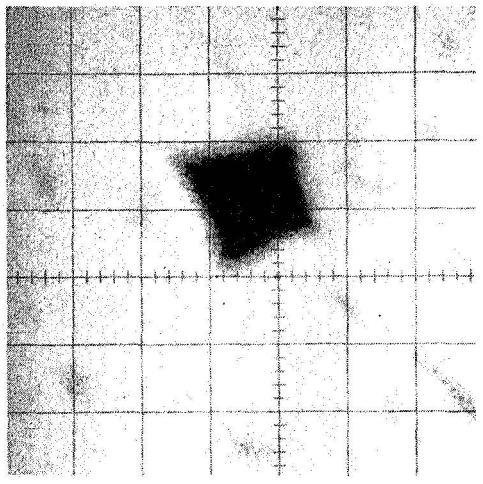

c. Chromium

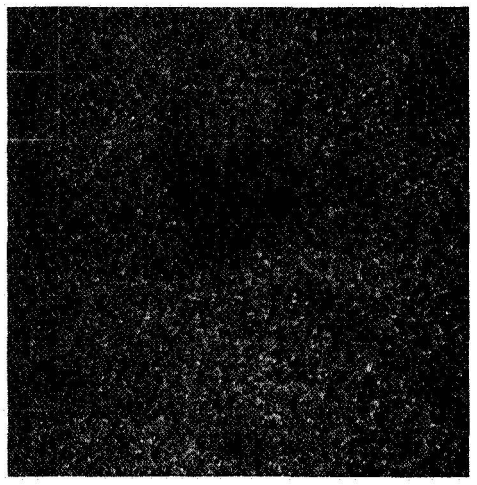

d. Silicon

Figure 9. X-ray images of the Fe, Co, Cr and Si radiation in the exploratory Fe - 50 Co base alloy. Bright areas show high concentrations of pertinent elements.

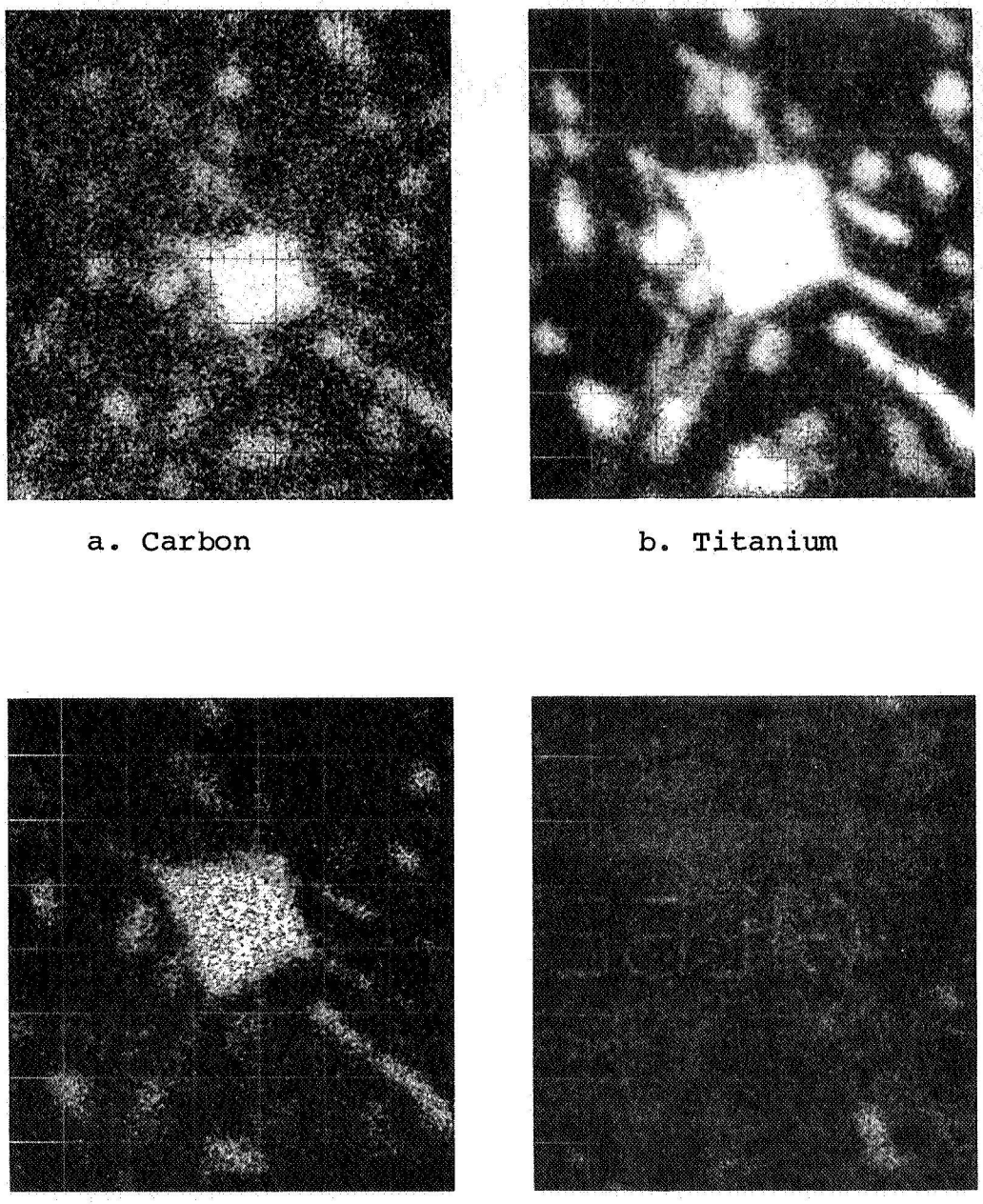

a. Carbon

b. Titanium

c. Tungsten

d. Zirconium

Figure 10. X-ray images of the C, Ti, W and Zr radiations in the exploratory Fe - 50 Co base alloy. Bright areas show high concentrations of pertinent elements.

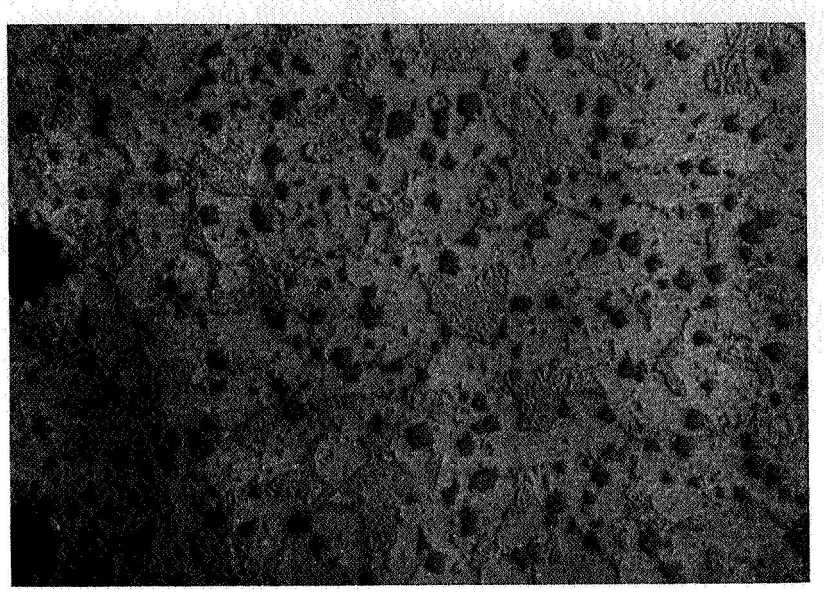

a. Untested

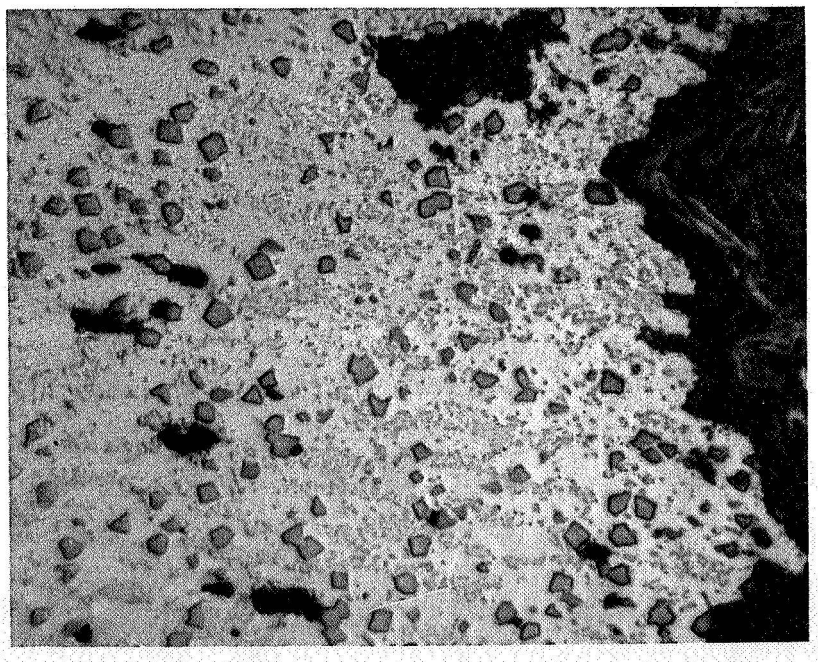

b. Tested

Figure 11. Microstructure of the exploratory Co-15 W base alloy. Direction of applied stress is horizontal. X250

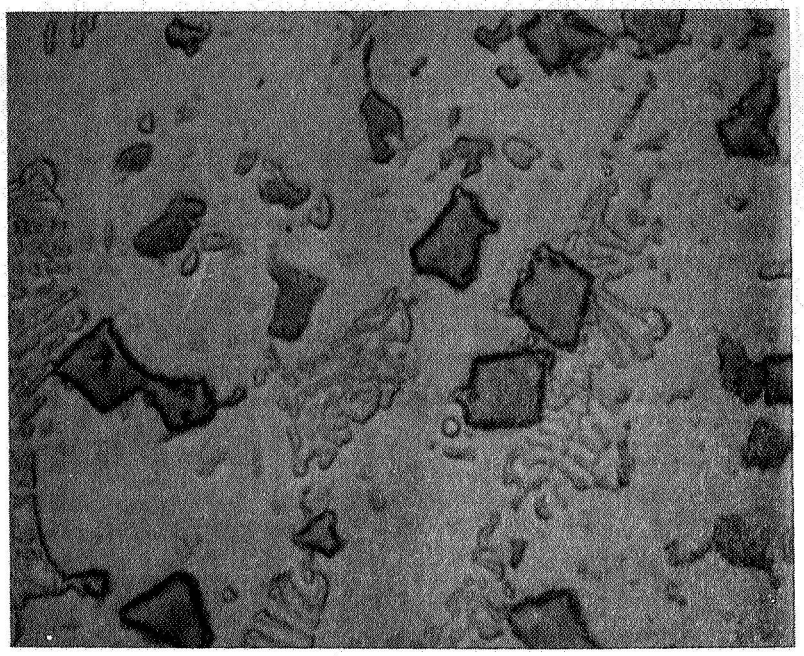

a. Microstructure

b. Tungsten

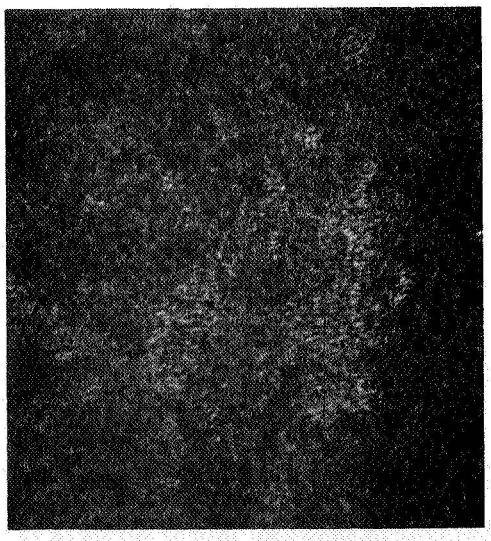

c. Molybdenum

Figure 12. Microstructure and x-ray images of the W and Mo radiations in the exploratory Co-15 W alloy. X1000

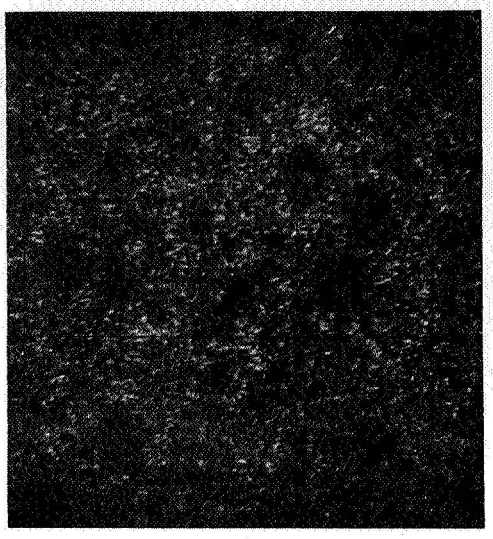

a. Silicon

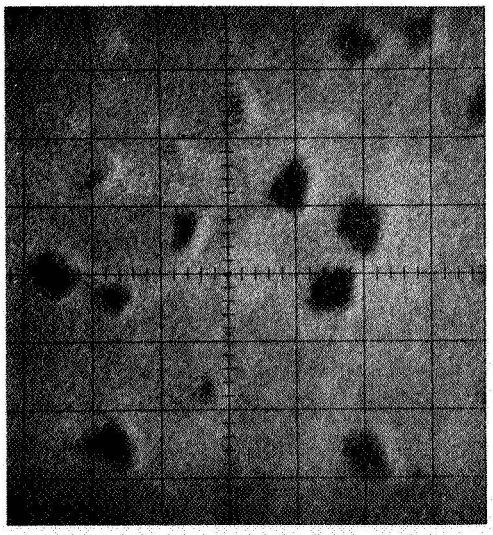

b. Cobalt

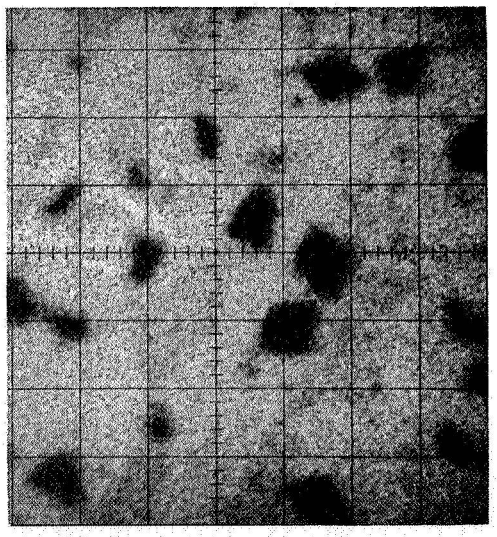

c. Chromium

Figure 13. X-ray images of the Si, Co and Cr radiations in the exploratory Co - 15 W base alloy.

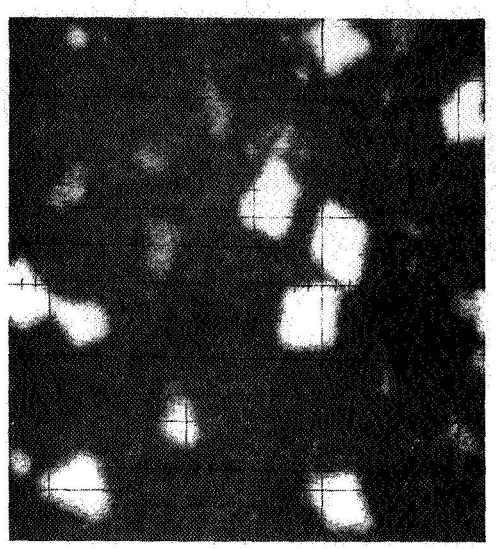

a. Titanium

b. Zirconium

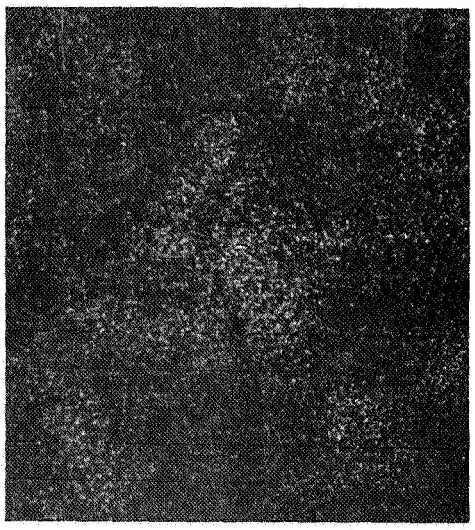

c. Boron

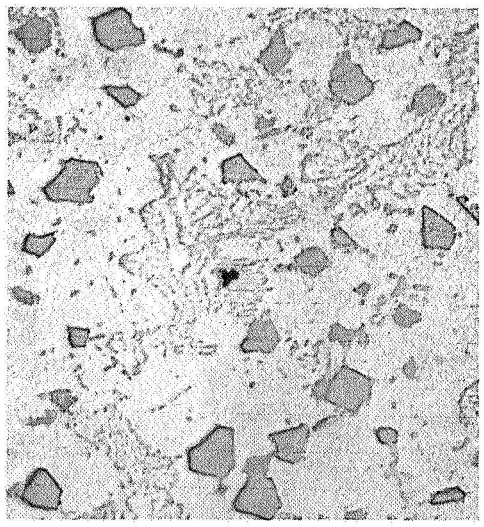

d. Microstructure corresponding to B image

Figure 14. X-ray images for the Ti, Zr and B radiations in the exploratory Co - 15 W base alloy.

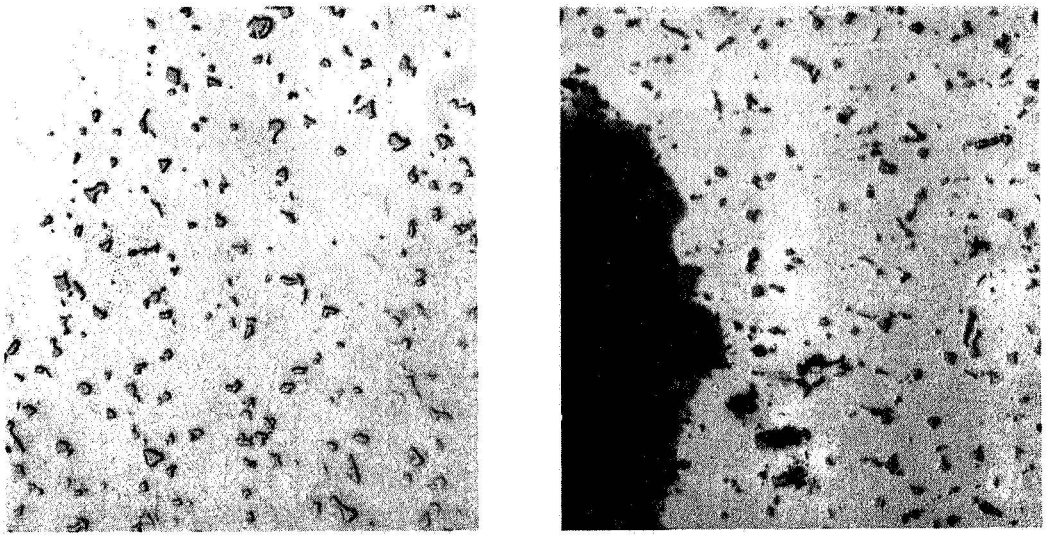

a. Untested b. Tested

Conventionally cast

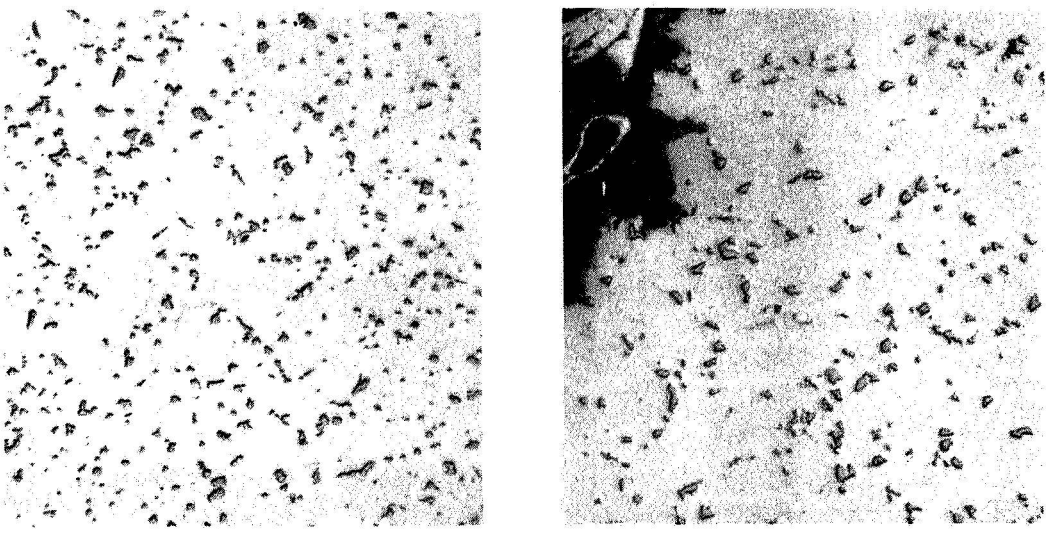

c. Untested d. Tested

Directionally cast

Figure 15. Microstructures of conventionally and directionally cast modified Fe - 50 Co base alloy. Direction of applied stress is horizontal. X250

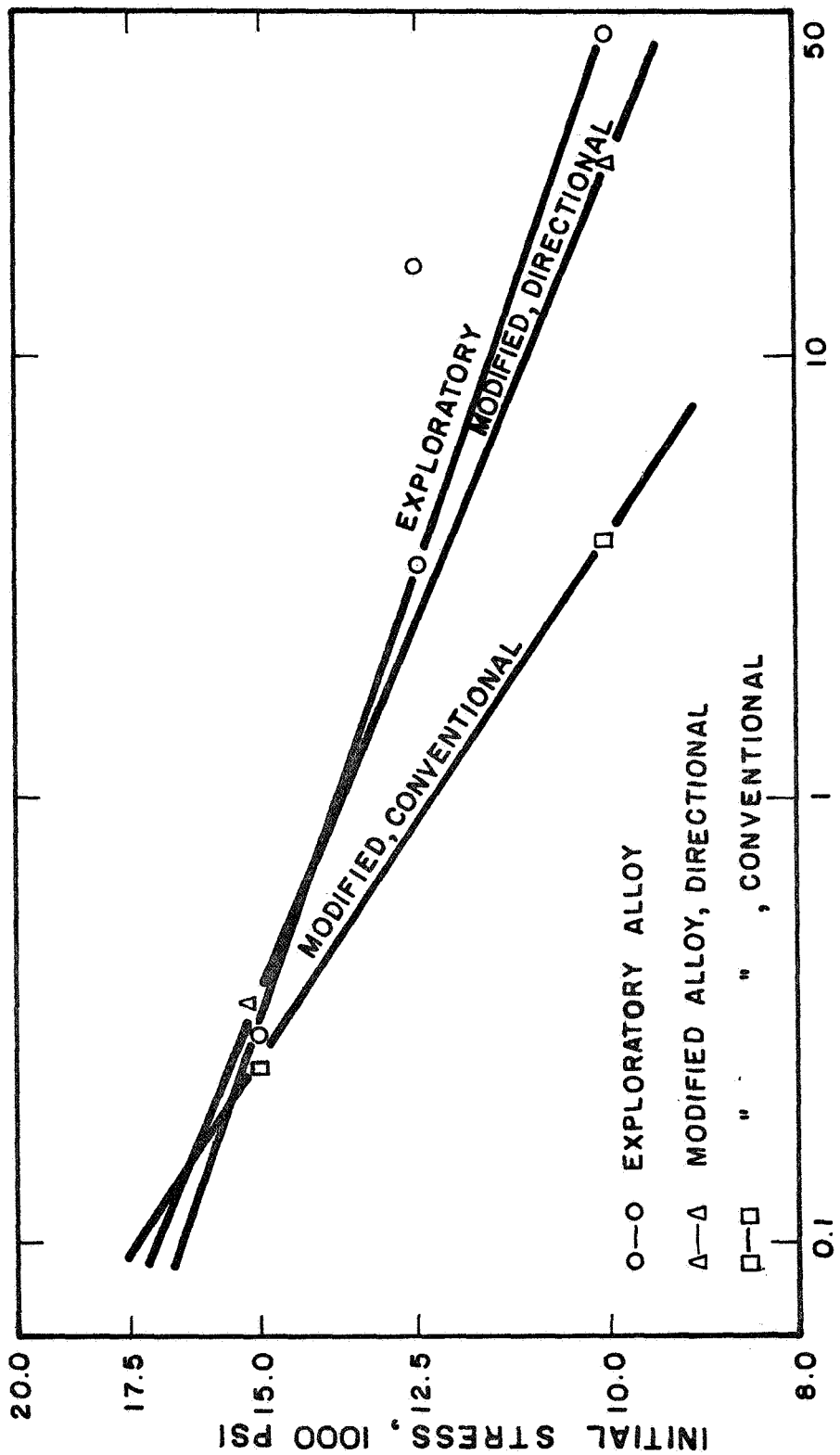

FIGURE 16. STRESS RUPTURE PROPERTIES OF THE Fe-50 Co BASE ALLOYS AT 1850°F IN AIR.

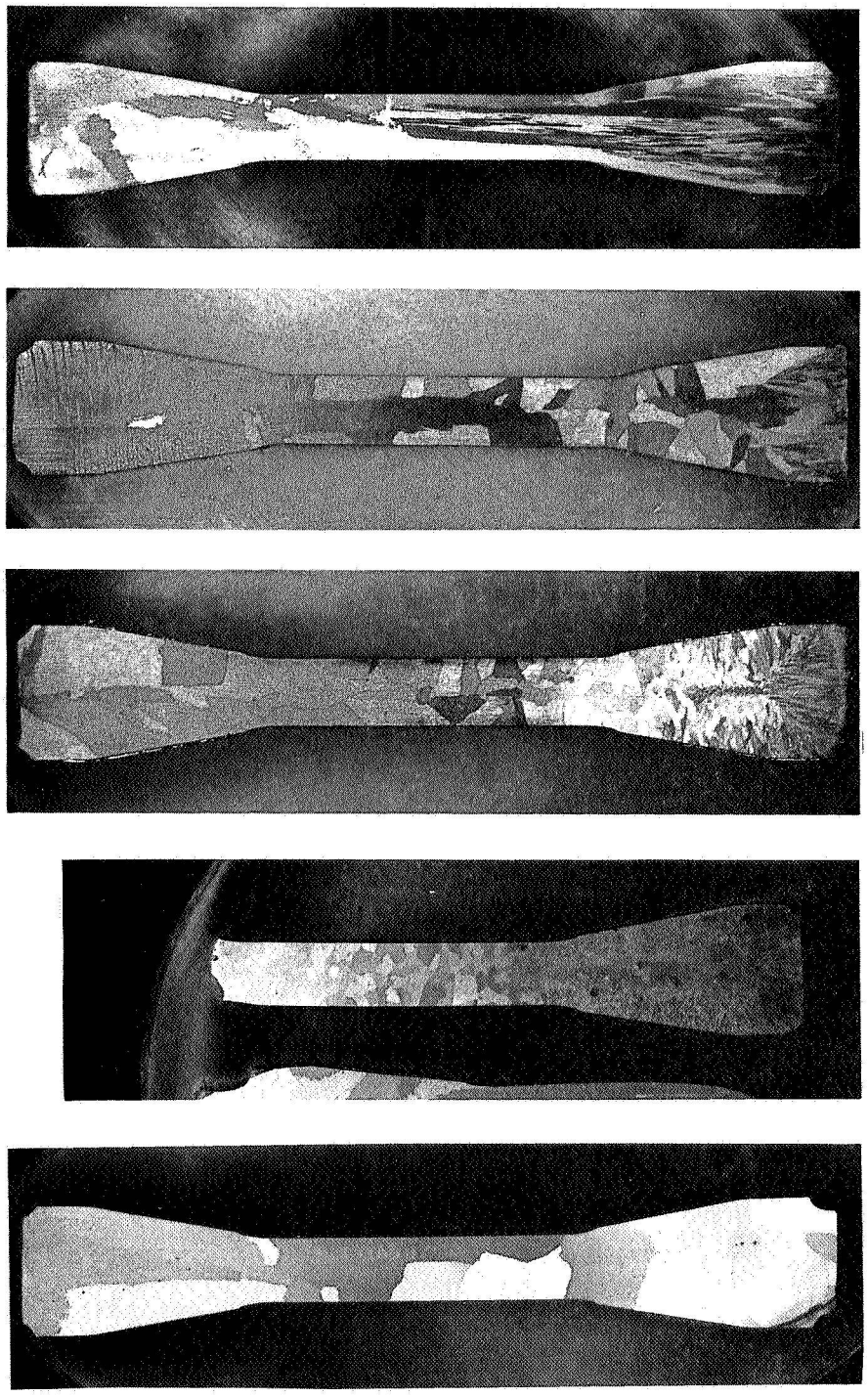

Figure 17. Typical macrostructures of as-cast stress rupture test bars.

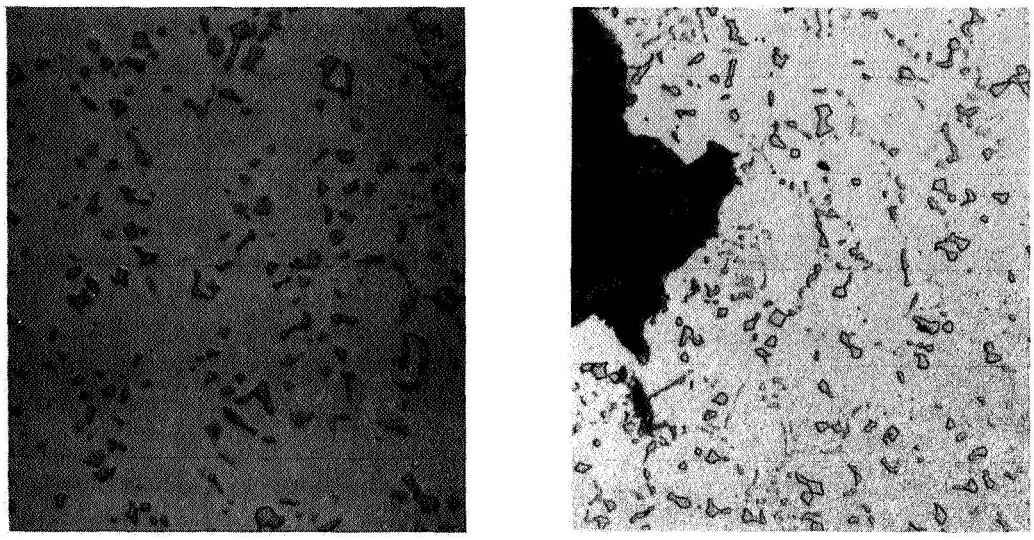

a. Untested b. Tested

Conventionally cast

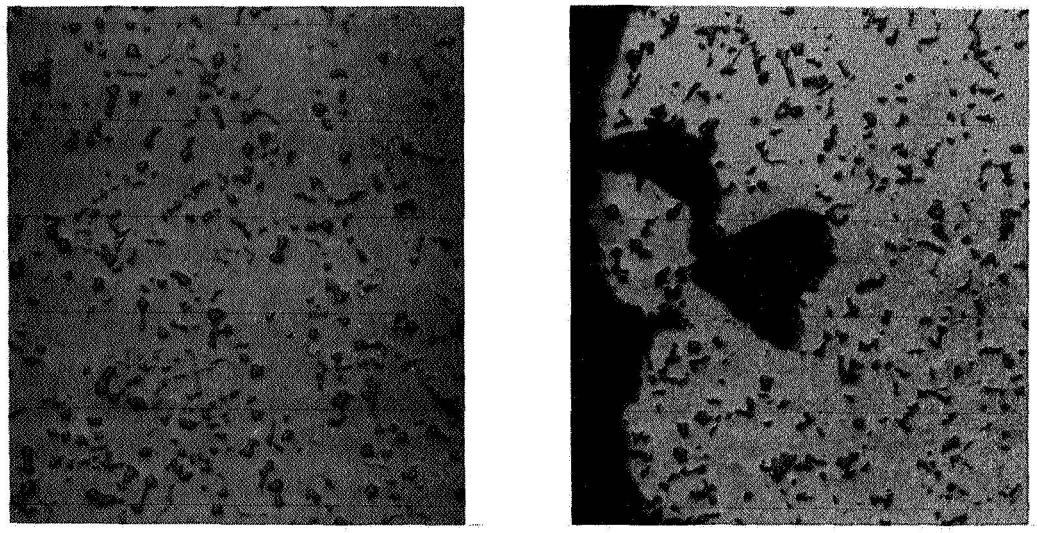

c. Untested d. Tested

Directionally cast

Figure 18. Microstructure of the conventionally and directionally cast Co - 15 W base alloy modified with 10 Cr, 2 Zr, 2 Ti and 1 C. X250

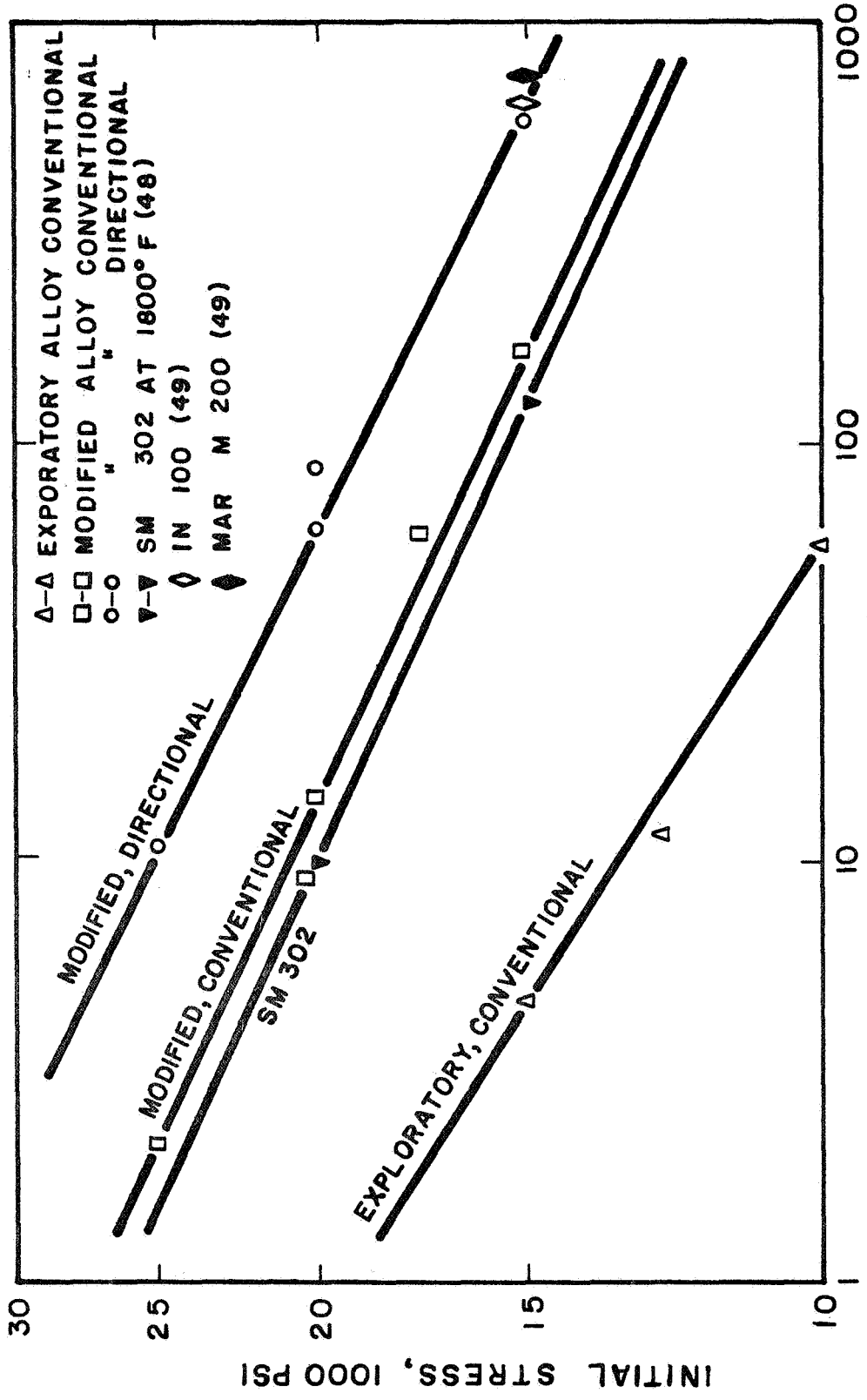

FIGURE 19. COMPARISON OF STRESS RUPTURE TEST RESULTS AT 1850°F IN AIR OF THE Co-15W BASE ALLOY WITH COMMERCIAL ALLOYS.

a. Microstructure X1000

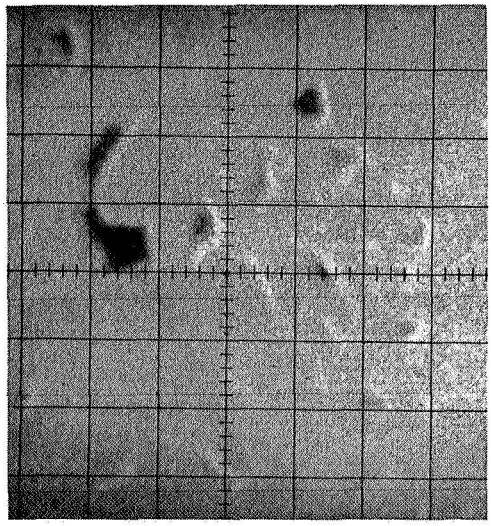

b. Cobalt

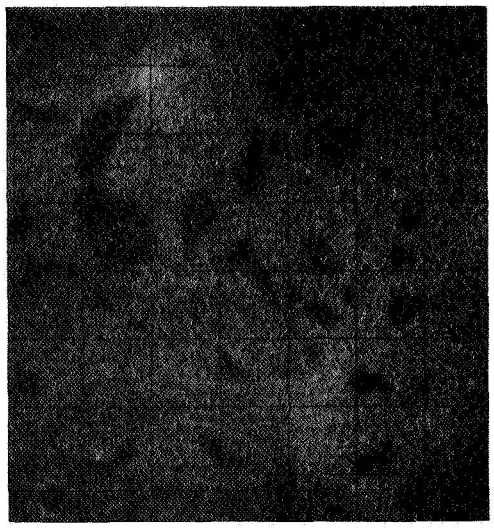

c. Chromium

Figure 20. Microstructure and x-ray images of the Co and Cr radiations in the conventionally cast modified Co - 15 W base alloy. Bright areas indicate high concentrations of the pertinent elements.

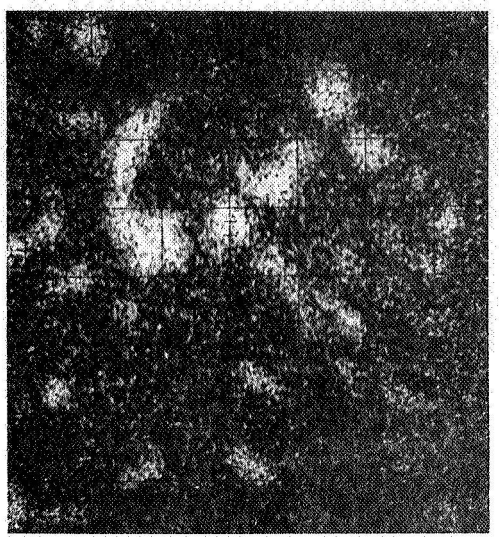

a. Tungsten

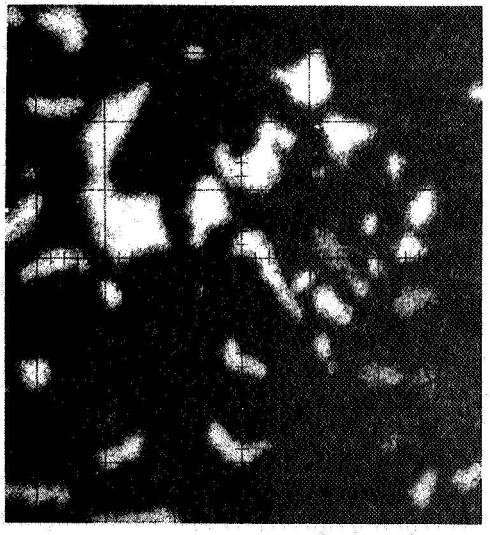

b. Titanium

c. Zirconium

Figure 21. X-ray images of the W, Ti and Zr radiations in the conventionally cast modified Co - 15 W base alloy. Bright areas indicate high concentrations of pertinent elements.

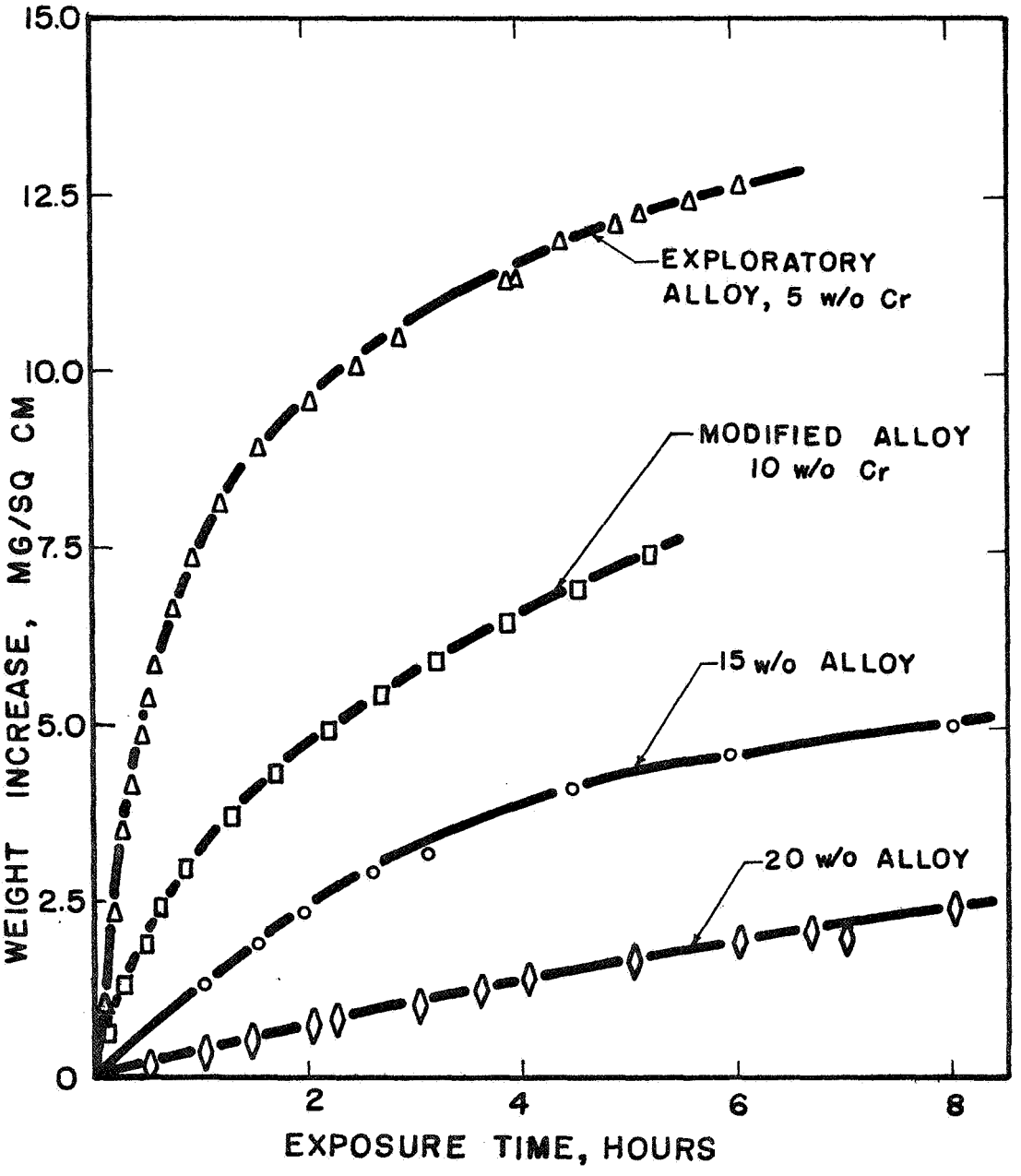

FIGURE 22: WEIGHT GAIN OF Co-15W BASE ALLOYS ON OXIDATION IN STILL AIR AT 1850° F.

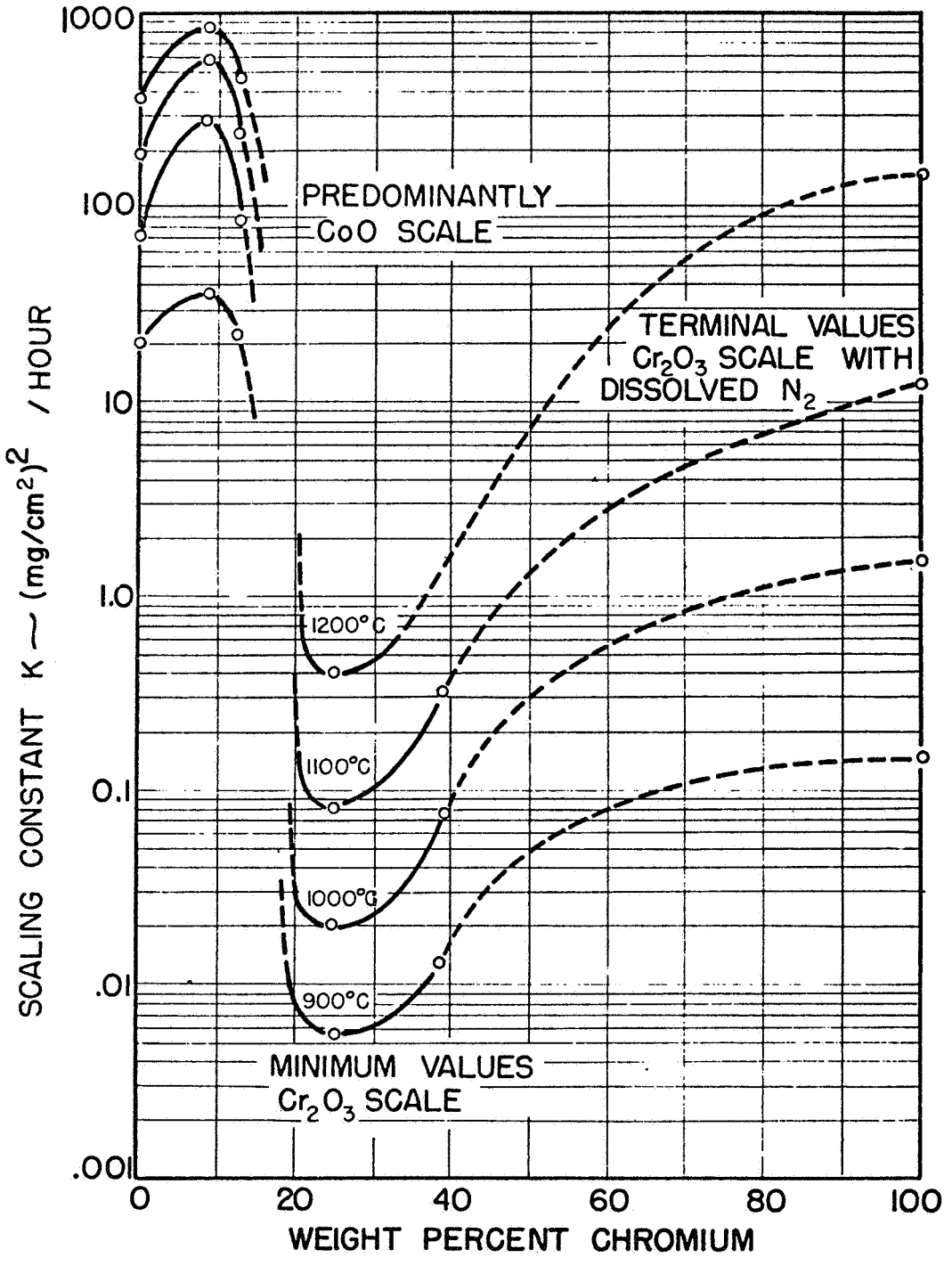

FIG. 23: FIRST PARABOLIC SCALING CONSTANT VS. ALLOY COMPOSITION FOR COBALT CHROMIUM ALLOYS HEATED IN AIR (50)

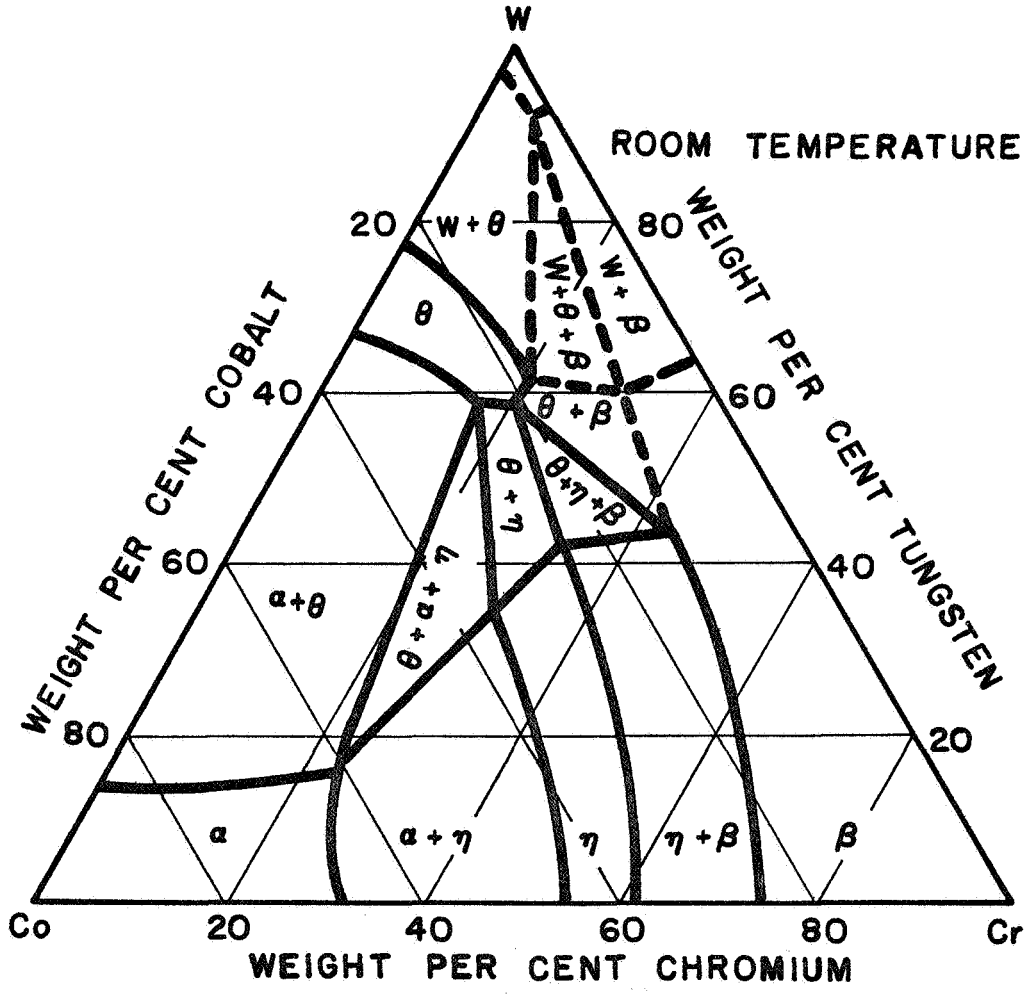

FIGURE 24: COBALT-TUNGSTEN-CHROMIUM TERNARY DIAGRAM (51)

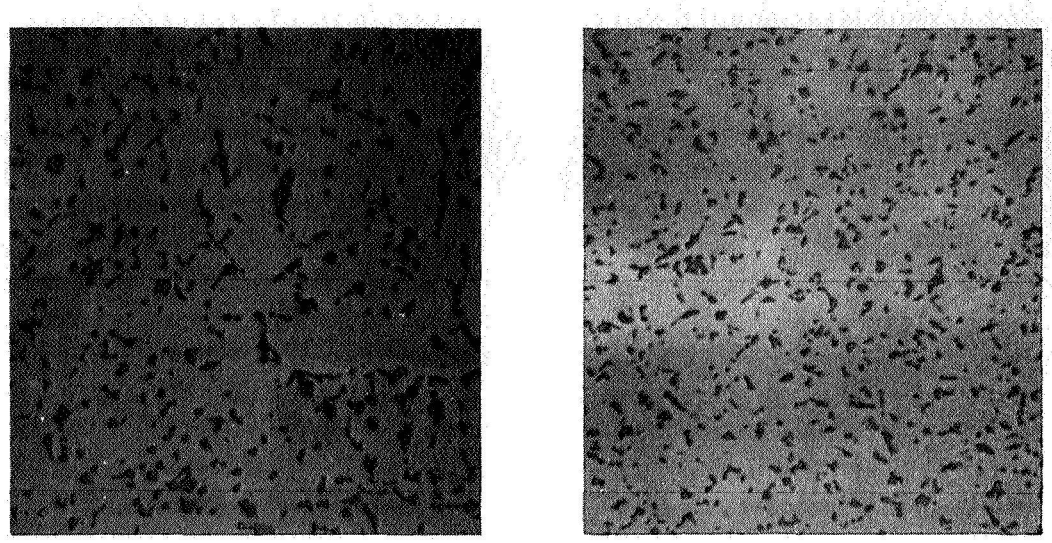

a. Conventional b. Directional

15 w/o Cr content

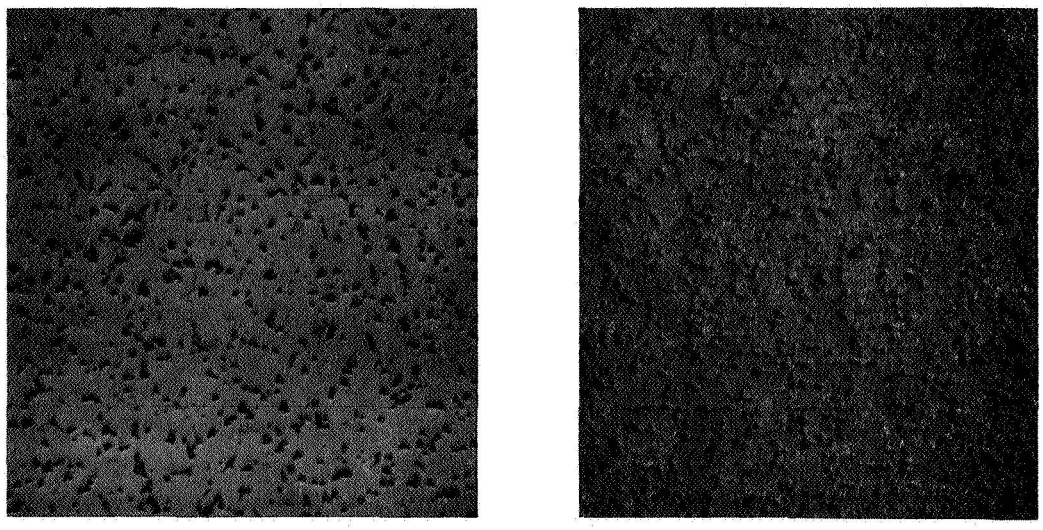

c. Conventional b. Directional

20 w/o Cr content

Figure 25. Microstructures of conventionally and directionally cast Co - 15 W, 2 Zr, 2 Ti 1 C base alloys with 15 w/o and 20 w/o Cr.

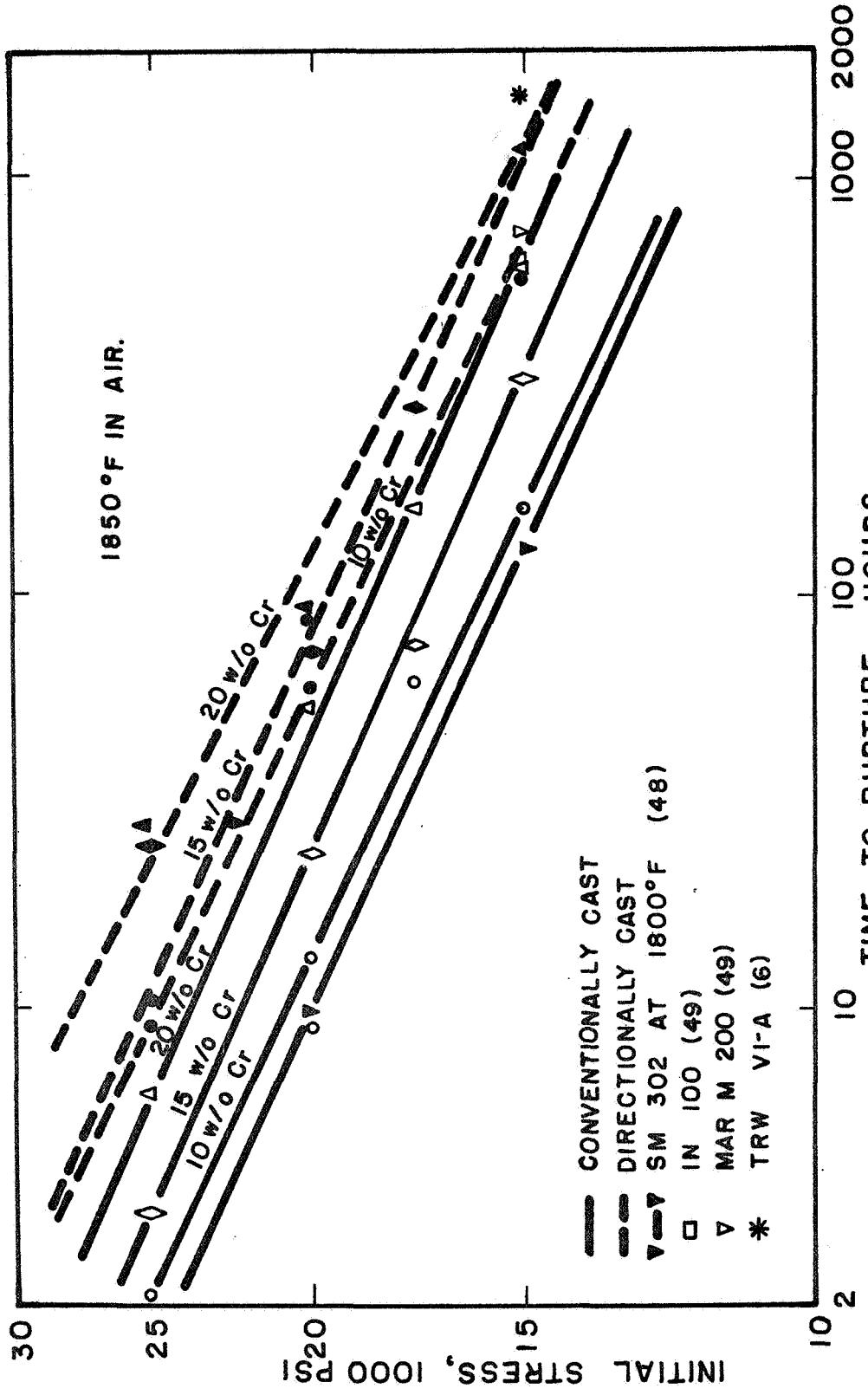

FIGURE 26. EFFECT OF INCREASING CHROMIUM CONTENT ON STRESS RUPTURE LIFE OF Co-15W BASE ALLOYS.

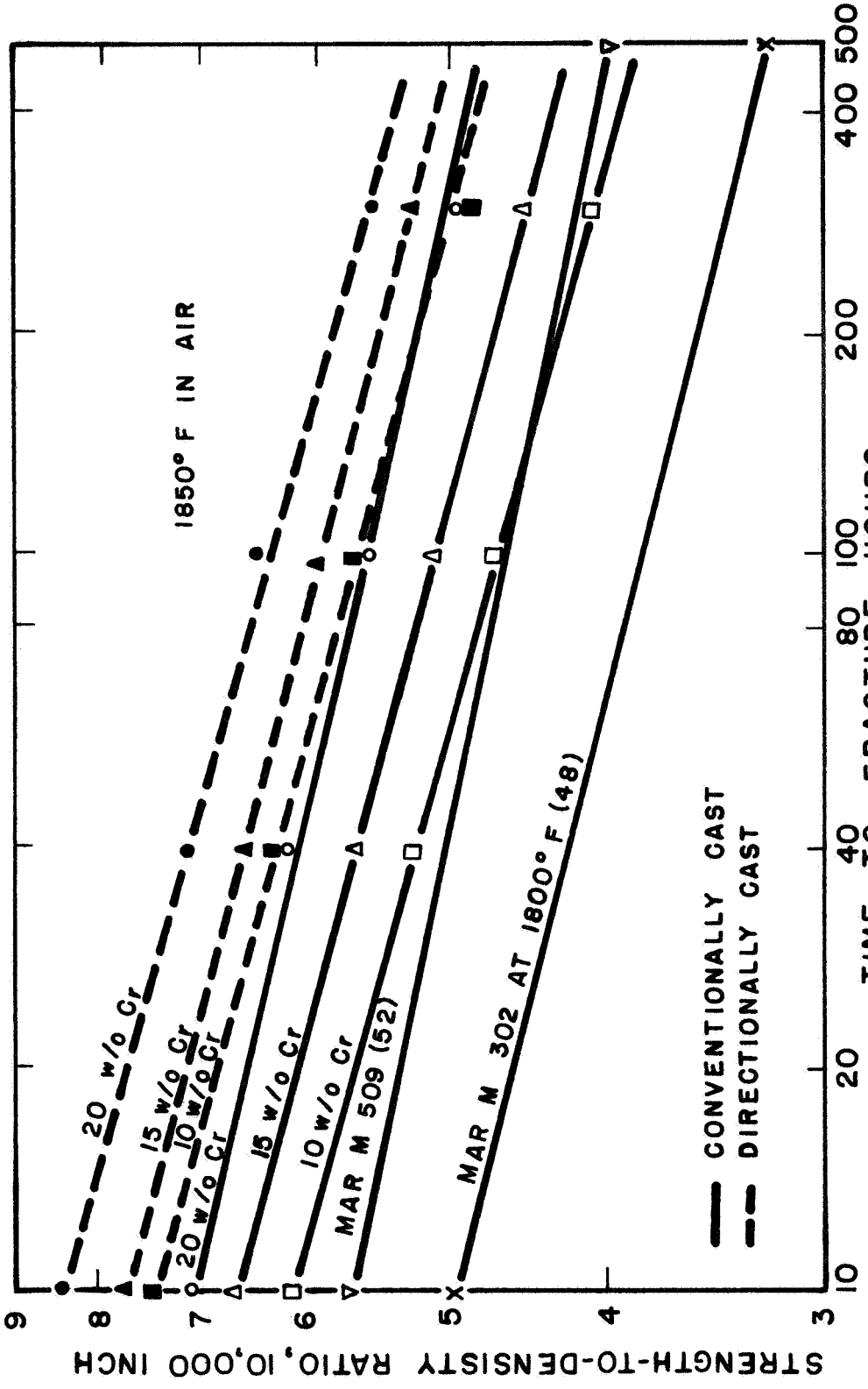

FIGURE 27. STRESS RUPTURE PROPERTIES OF Co-15 W, 2 Zr, 2 Ti, IC BASE ALLOY ON A STRENGTH-TO-DENSITY RATIO BASIS.

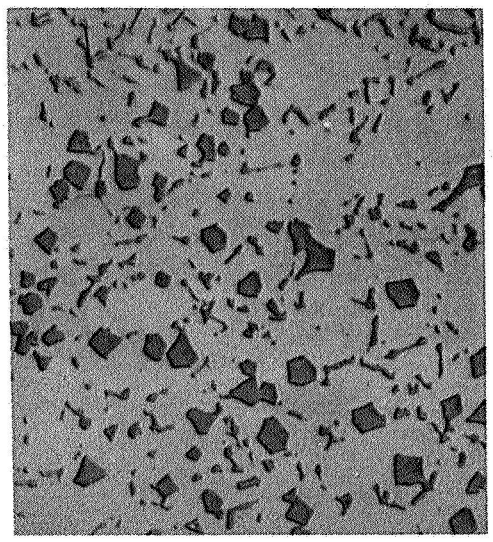

a. With 3 Zr, 3 Ti, 1.5 C conventionally cast

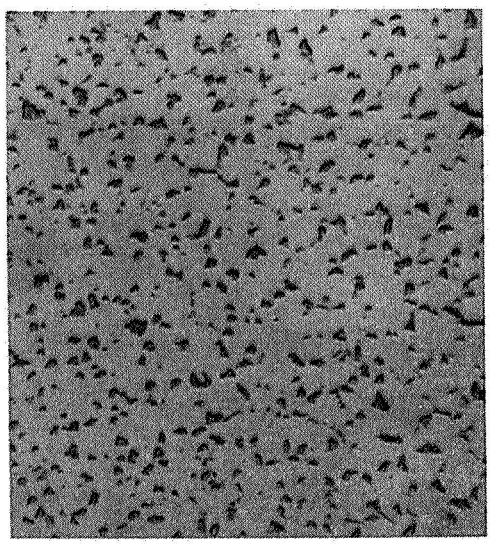

b. With 15 Cr, 3 Zr Directionally cast

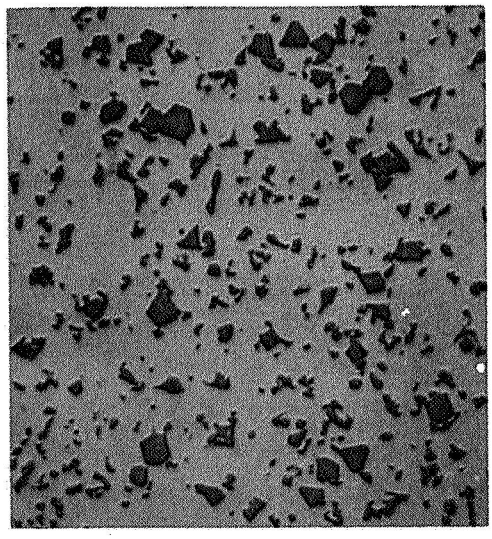

c. With 15 Cr, 3 Zr, 3 Ti, 1.5 C; conventionally cast

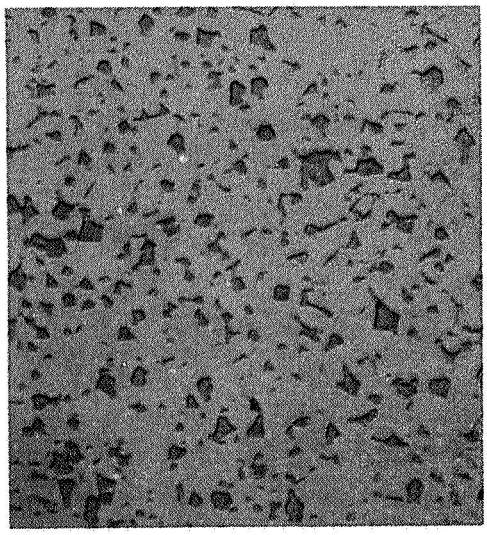

d. With 15 Cr, 3 Zr, 3 Ti, 1.5 C; directionally cast

Figure 28. Microstructures of Co - 15 W base alloys with increased Zr, Ti and C contents.

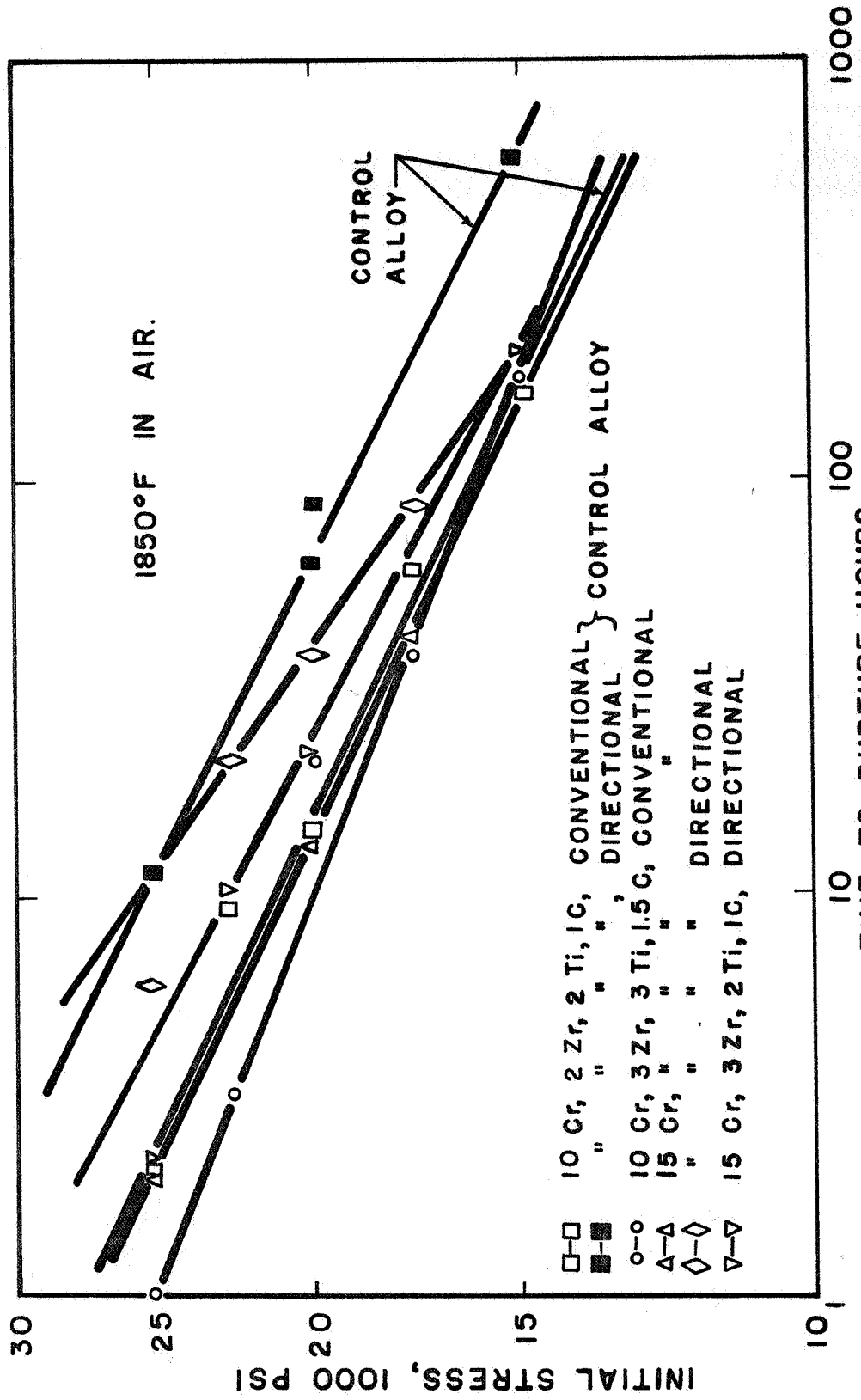

FIGURE 29. EFFECT OF Zr AND Ti ON 1850°F STRESS RUPTURE LIFE OF Co-15W BASE ALLOYS

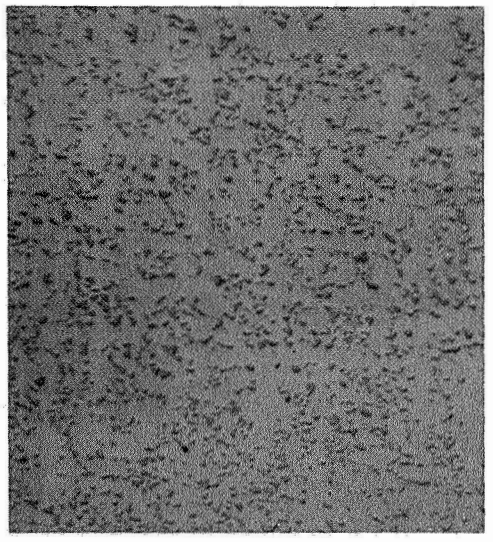

a. 80 F mold

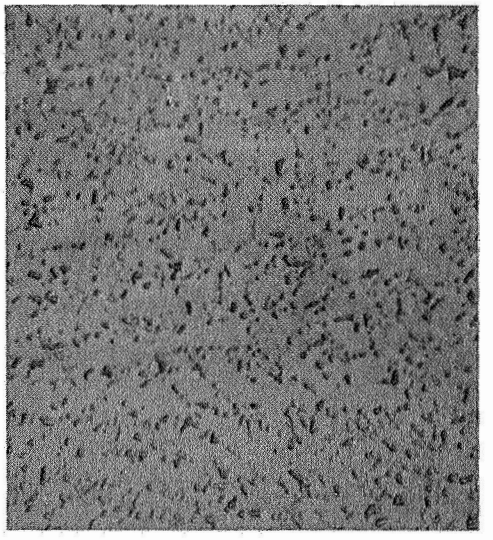

b. 1000 F mold

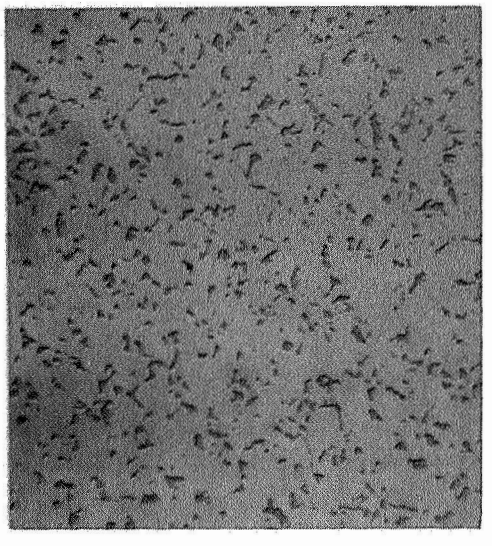

c. 1600 F mold

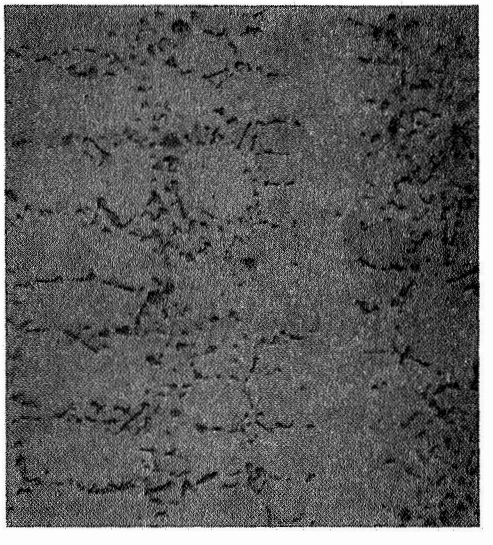

d. 2320 F mold

Figure 30. Microstructures of Co - 15 W, 15 Cr, 2 Zr, 2 Ti, 1 C alloy directionally cast at different mold temperatures. X250

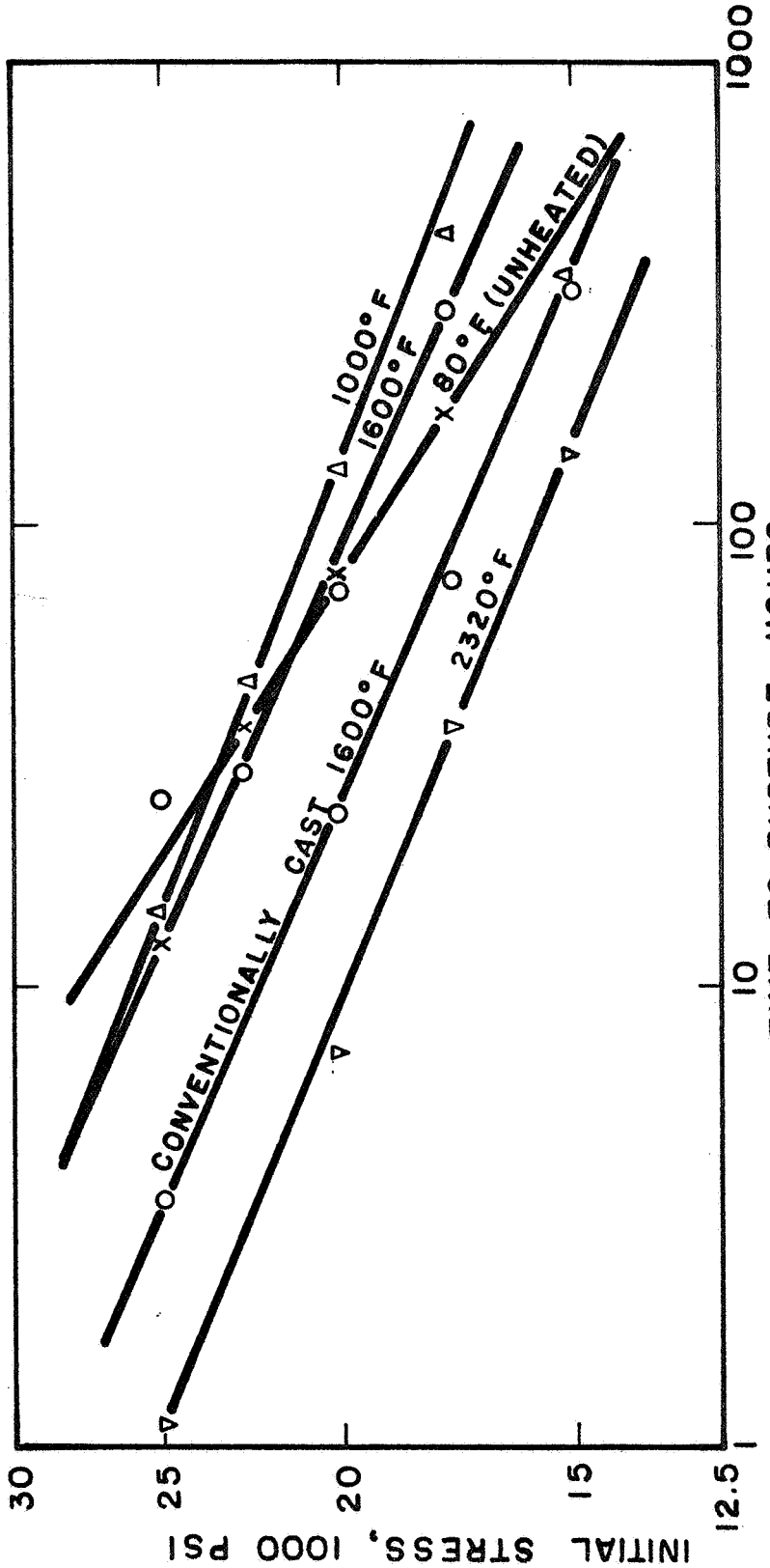

FIGURE 31. EFFECT OF MOLD TEMPERATURE ON 1850° F STRESS RUPTURE LIFE IN AIR OF DIRECTIONALLY CAST Co-15W, 15Cr, 2Zr, 2Ti, IC ALLOY.